Università degli studi di Milano-Bicocca

Department of Biotechnologies and Biosciences

PhD Program in Molecular and Translational Medicine

(DIMET)

Arrhythmogenic mechanisms in genetic channelopathies

Candidate:

Joyce Bernardi (Matr. 787784)

Tutor: Prof. Antonio Zaza, MD

Coordinator: Prof. Andrea Biondi, MD

XXIX cycle

Academic Year 2015-2016

Contents

Chapter 1

Introduction

Acronyms

AP	action potential
APD	action potential duration
ECG	electrocardiogram
ECC	excitation-contraction coupling
I_{CaL}	L-type Ca^{2+} current (LTCC)
I_{Kr}	rapidly activating delayed rectifier potassium channels
I_{Ks}	slowly activating delayed rectifier potassium channels
LQT1	long QT syndrome type 1
LQTS	long QT syndrome
NO	nitric oxide
NOS	nitric oxide synthase
NOS1AP	nitric oxide synthase adaptor protein 1
PLB	phospholamban
PMCA	plasma membrane Ca^{2+}-ATPase
QTc	corrected QT interval
RyR	ryanodine receptor
SCD	sudden cardiac death
SERCA	sarcoplasmic reticulum Ca^{2+}-ATPase
SNP	single nucleotide polymorphism
SR	sarcoplasmic reticulum

Myocardial repolarization is a complex phenomenon, generated by the interplay of several ionic currents. The duration of repolarization differs among cardiac regions with a well defined pattern, such as that, in spite of their different activation times, all regions may repolarize almost simultaneously (wihin a narrow time window). If such a pattern is perturbed, arrhythmias may occur. Accordingly, repolarization duration and stability (in time and space) are of pivotal importance in maintaining the physiological electrical activity. Understanding the mechanisms underlying repolarization abnormalities may identify targets for arrhythmia prevention and biomarkers suitable to risk stratification in conditions leading to sudden cardiac death.

During my thesis work I addressed two aspects of cardiac repolarization abnormalities. The first study, to which I collaborated as junior PhD student, systematically analyzed how gating abnormalities of I_{Kr} may affect ventricular repolarization and its temporal stability. This study exploited the innovative technique of "Dynamic Clamp", obtaining results relevant to the understanding of arrhythmogenesis in I_{Kr} channellopathy (LQT2 syndrome). The second study, of which I was in charge as principal investigator, addressed the mechanism underlying the role of polymorphisms of NOS1AP, encoding for the NOS1-anchor protein CAPON, in determining the phenotype of I_{Ks} channellopathy (LQT1 syndrome). The results obtained indicate that, when interacting with prolonged repolarization (as in LQT1), NOS1 loss of function may cause substantial instability of intracellular Ca^{2+} handling and the resulting electrical disturbances.

Because of my primary role in it, I will expand here on the LQT1 study and then more succinctly summarize the LQT2 one. Presentation of the actual works will be preceded by an introduction to the topics most relevant to the area of the two studies and required for understanding the results obtained.

1. Long QT syndrome (LQTS)

The long QT syndrome (LQTS) is an heterogeneous disorder of myocardial repolarization characterized by a prolongation of QT interval on the electrocardiogram (ECG) and clinically manifested with syncopal episodes and seizures, that may lead to cardiac arrest and sudden cardiac death as consequences of physical or emotional stress [1]. Two hereditary variants of LQTS have been described: the extremely severe, autosomal recessive, Jervell and Lange-Nielsen syndrome (JLNS), associated with deafness; and the most common, autosomal dominant, Romano-Ward syndrome (RWS) [2]. Mutations in at least 13 genes encoding ion cardiac channel subunits or proteins involved in modulating ionic currents have been identified, but the majority of LQTS cases (90%) show mutation in three of them: KCNQ1 (LQT1), KCNH1 (LQT2) and SCN5A (LQT3) [3] (**Table 1**). Disease prevalence is estimated at close to 1 in 2,500 live births [4]. Mutation type, location, and even a patient's ethnic background, age, and gender are critical factors that affect the pathophysiology of the disease [3]. Traditionally, QTc values > 440 ms are considered prolonged; however, values up to 460 ms may still be normal among females, suggesting a role for hormonal changes [5]. Anyway, there are exceptions, as syncopal episodes can occur also in patients with modest QT prolongation and even with a normal QT interval, but in general, with a longer QT the risk for malignant arrhythmias is greater, and evidences indicate that when the QTc exceeds 500-550 ms there is a definite increase risk [6].

Gene	Syndrome	Frequency	Locus	Protein (Functional Effect)
KCNQ1 (**LQT1**)	RWS, JLNS	40–55	11p15.5	Kv7.1 (↓)
KCNH2 (**LQT2**)	RWS	30–45	7q35–36	Kv11.1 (↓)
SCN5A (**LQT3**)	RWS	5–10	3p21–p24	NaV1.5 (↑)
ANKB (**LQT4**)	RWS	<1%	4q25–q27	Ankyrin B (↓)
KCNE1 (**LQT5**)	RWS, JLNS	<1%	21q22.1	MinK (↓)
KCNE2 (**LQT6**)	RWS	<1%	21q22.1	MiRP1 (↓)
KCNJ2 (**LQT7**)	AS	<1%	17q23	Kir2.1 (↓)
CACNA1C (**LQT8**)	TS	<1%	12p13.3	$Ca_V1.2$ (↑)
CAV3 (**LQT9**)	RWS	<1%	3p25	Caveolin 3 (↓)
SCN4B (**LQT10**)	RWS	<1%	11q23.3	Na^+ channel-β4 (↓)
AKAP9 (**LQT11**)	RWS	<1%	7q21–q22	Yotiao (↓)
SNTA1 (**LQT12**)	RWS	<1%	20q11.2	Syntrophin α1 (↓)
KCNJ5 (**LQT13**)	RWS	<1%	11q24	Kir3.4 (↓)

Table 1. LQTS genes. RWS: Romano-Ward syndrome; JLNS: Jervell-Nielsen syndrome; AS: Andersen syndrome. TS: Timothy syndrome. Functional effect: (↓) loss-of-function or (↑) gain-of-function at the cellular in vitro level. Adapted from [3].

There is a significant number of silent mutation carriers (QTc < 440 ms) that actually ranges between 10% and 36% according to genotype [6, 7] as a consequence of low penetrance. Therefore, along with the standard diagnostic criteria (first proposed in 1985 and subsequently updated, listed in **Table 2**), molecular and genetic screening has now become essential in the diagnosis of borderline cases and to identify potential silent mutations in family members [8].

1.1 Management and Therapies

The trigger for most of the episodes of life-threatening arrhythmias of LQTS is represented by a sudden increase in sympathetic activity, largely mediated by quantitatively dominant left cardiac sympathetic nerves [9], therefore β-adrenergic blocking agents represent the first choice therapy in symptomatic LQTS patients. In patients where this treatment is not effective, the removal of the first four thoracic ganglia, known as Left Cardiac Sympathetic Denervation (LCSD), is indicated as a second choice. This procedure leads to a consequent reduction in noradrenaline release at ventricular level without decreasing the heart rate and a significant shortening of the QTc [9]. However, in case of a documented cardiac arrest, either on or off antiadrenergic therapy (β-blockade and LCSD), an Implantable Cardioverter Defibrillator (ICD), which generates electrical shocks to restore the normal electrical activity during arrhythmias, should be implanted.

ECG findings		**Points**
QTc	> 480 ms	3
	460 – 470 ms	2
	450 – 459 (male) ms	1
QTc 4th minute of recovery from exercise stress test ≥ 480 ms		1
Torsade de Pointes (TdP)		2
T Wave alternans		1
Notched T waves in 3 leads		1
Low heart rate for age		0.5
Clinical History		
Syncope with stress		2
Syncope without stress		1
Congenital deafness		0.5
Family History		
Family members with definite LQTS		1
Unexplained SCD below age 30 among immediate family members		0.5

Table 2. 1993-2006 Long QT syndrome (LQTS) diagnostic criteria. QTc calculated by Bazett's formula where QTc = QT/√RR. Relative points assigned to various electrocardiographic, clinical and familiar findings. The score range from a minimum value of 0 to a maximum value of 9 points. Score and probability categories: ≤ 1 point = low probability; > 1 to 3 points = intermediate probability, and ≥ 3.5 points = high probability of LQTS. Adapted from [9].

1.2 Long QT syndrome type 1 (LQT1)

LQT1 is the most common form of LQTS and is caused by mutations in KCNQ1, a gene encoding the α-subunit of the slow component of delayed rectifier K^+ current (I_{Ks}) channel [9]. The channel carries the major outward repolarizing K^+ current during the plateau phase of cardiac action potentials (APs) and plays a critical role in maintaining repolarization reserve in the heart [10]. Under normal physiological conditions, sympathetic activation promotes I_{Ks}, which shortens ventricular repolarization against the activation of L-type Ca^{2+} current and thereby protects against Ca^{2+}-related arrhythmogenicity [10]. In a condition of I_{Ks} defect, as due to a KCNQ1 mutation, the ventricular repolarization or QT interval fails to shorten appropriately, thus creating a highly arrhythmogenic condition [3]. In human ventricular myocytes, the slow and rapid component of delayed rectifier K^+ current (I_{Ks} and I_{Kr}, outward currents), together with L-type Ca^{2+} current I_{CaL} (inward current) play a dominant role in the repolarization of APs and are the most important determinants of AP duration (APD). Under physiological conditions, I_{Kr} and I_{CaL}, but not I_{Ks}, normally are crucial in controlling the ventricular AP at rest [11]. Therefore, one possible explanation for individuals carrying a KCNQ1 mutation which display a silent phenotype may be the "repolarization reserve" mechanism [12]. On the other hand, I_{Ks} plays a major role in regulating the ventricular AP after adrenergic stimuli, that upregulates I_{Ks} through cAMP-dependent PKA pathway to prevent excessive ventricular APD or QT prolongation due to an I_{CaL} increase [13, 14].

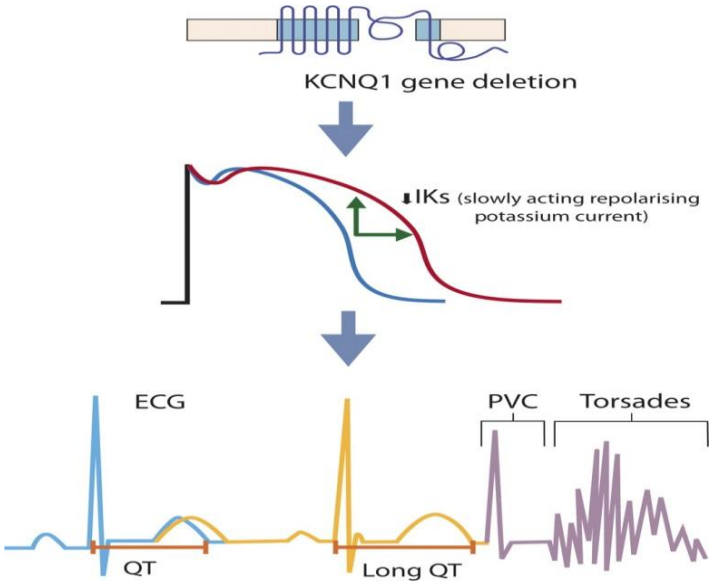

Figure 1. The gene deletion in LQT1 (KCNQ1) leads to a reduction in the repolarizing potassium current (I_{Ks}) and prolongation of repolarization, consequently lengthening the QT interval. A premature ventricular contraction (PVC) occurring during the vulnerable part of repolarization leads to establishment of polymorphic ventricular tachycardia (Torsades de Pointes). From [15].

2. Repolarization reserve and intrinsic QT variability in Long QT syndrome

The concept of repolarization reserve was first proposed, and defined by Roden, [16] and has been demonstrated experimentally by other researchers [17-20]. Normal cardiac repolarization critically depends on the interplay of multiple ion currents, and these provide some redundancy or "reserve", therefore, pharmacological, congenital or acquired impairment of one type of transmembrane ion channel does not necessarily result in overt repolarization changes because other

repolarizing currents can take over and compensate. This mechanism protects against QT prolongation and allows for an LQTS mutation to remain clinically silent or mild. The lesions in this repolarizing mechanism can reduce "repolarization reserve" and therefore increase the risk for marked AP prolongation and arrhythmias, as when a pathologic trigger such as an I_{Kr}-blocking medication is superimposed [21].

Beat-to-beat variability of repolarization duration (BVR) is an intrinsic characteristic of cardiac function that can be observed at multiple levels, from temporal variations in AP duration (APD) of the single cardiac myocyte or of the QT interval on the body-surface ECG (QTV) [22-24]. Repolarization variability is considered a better marker of proarrhythmia than repolarization prolongation alone in various experimental models of TdP ventricular tachycardia [25-27] and in human cardiac pathologies [23, 28]. In fact, increased BVR (and QTV) is generally associated to impaired repolarization [29, 30] and has been linked with ventricular arrhythmias or sudden death [31, 32].

Therefore, understanding the ionic mechanisms underlying BVR in isolated cells may therefore help to inform the use of BVR as an arrhythmic risk biomarker (for example for drug testing), and also to better understand its causal relationship with arrhythmia [33, 34].

3. Genetic modifiers of the Long QT syndrome

The evidence of variable clinical manifestations in patients with the same genetic defect was first reported several years ago by Priori and

colleagues [7]. The occurrence of a LQTS mutation without clinical signs of the disease is relatively common (10-35%); furthermore, LQTS mutations have been indentified in 8-10% of patients who show QT prolongation and arrhythmias only upon exposure to QT prolonging drugs, without spontaneous clinical manifestation [35]. This variable expressivity limits the predictive value of genotyping. In the absence of obvious exogenous cause of QT abnormality, genetic modifiers become the most plausible candidates to account for the weak genotype-phenotype correlation [36].

In an attempt to identify the genetic components of clinical variability several hypothesis have been addressed. Firstly, the role of compound/double heterozygosity has been considered, in view of the possibility that a concurrent, or "second hit", mutation may contribute to disease severity. As a second line of research has addressed the role of non-synonymous common gene variants (nsSNPs), phenotypically inconsequential per se, but liable to worsen (or attenuate) the effect of the signal mutation. Some among them, are reported to affect QTc and/or sudden cardiac death (SCD) risk even in the general population and, because of this are of particular interest in the context of LQTS. So far, variants of the NOS1AP gene has been consistently found to correlate with QT interval in healthy subjects [37]. Furthermore, NOS1AP variants are also an independent predictor of cardiac events in patients with mild QTc prolongation (<500 ms), whose risk stratification proves most difficult [38]. The risk of events is already so high in patients with more pronounced QTc prolongation that the presence of a SNP is unlikely to further modulate it. Overall, three NOS1AP SNPs (rs12029454, rs16847548, rs4657139) have been

associated with a longer QTc and four with an increased risk of cardiac events (rs12143842, rs16847548, rs10494366, rs4657139). Interestingly, at least two SNPs (rs12143842 and rs10494366) are predictors of events independently from the QTc [38, 39]. To add to the complexity, it has been reported that specific SNPs may have different effects (i.e. worsening or improving) in the presence of different mutations or according to their allelic position (cis, trans). In this context, demographic variables like gender and age may influence the risk of events, and represent additional modulators and further interactions with the genetic modifiers [36]. Taken together all these aspects, as of today, the only SNPs whose predictive value has been confirmed by independent investigations, and could thus be useful in risk stratification, are those occurring in the NOS1AP gene, perhaps the genetic locus with the largest effect size. Notably, NOS1AP variants associated with the QT interval are located in non-coding regions of the gene and may therefore affect the action of cis-acting elements (i.e. nuclear transcription factor) [40]. Eijgelsheim M, et al. looked for potential transcription-factors binding sites at the 5' region containing the SNP rs12143842 and reported that the C-to-T substitution resulted in two changes in predicted transcription factor binding sites [41]. Different studies did not identify any missense mutations in NOS1AP exons [42-44].

4. NOS1AP and NOS1 activity in the heart

The NOS1AP (nitric oxide synthase 1-adaptor protein) gene encodes for CAPON protein, first identified in the brain as a binding partner of

neuronal nitric oxide synthase (NOS1) [45]. CAPON is a highly conserved protein and at least two alternative isoforms are expressed [46]: CAPON long (~50 kDa), when all 10 exons are translated in protein; and CAPON short (~30 kDa), after the transcription of the last two exons only. The full-length isoform contains two distinguishable domains, the C-terminal PDZ (Postsynaptic density-95/Drosophila discs large/Zona occludens-1) domain, which is responsible for the interaction with NOS1; and a N-terminal phosphotyrosine-binding (PTB) domain [47]. Within the myocardium there are three distinct isoforms of NO synthase (NOS) which synthesize NO upon the cleavage of L-arginine into L-citrulline [48, 49]: neuronal NOS (nNOS, NOS1), inducible NOS (iNOS, NOS2) and endothelial NOS (eNOS, NOS3). NOS1 and NOS3 are constitutively expressed and produce NO in phase with myocyte contraction because they are activated by the Ca^{2+}-calmodulin complex. Although NO is a highly diffusible signaling molecule, signaling via NOS1 and NOS3 is compartmentalized, and NOS1 and NOS3 differentially modulate cardiac function [48, 50, 51]. The rate of synthesis of NO by NOS1 is 6 times that of NOS3 [52]. NOS2, on the other hand, is only expressed during inflammatory responses, and when expressed, produces much higher levels of NO independent of intracellular Ca^{2+} concentration, compared to the constitutive NOS isoforms [49, 53], thus resulting in signaling that is not compartmentalized. Of the three isoforms, only NOS1 contains a PDZ domain, therefore CAPON interacts with NOS1 but not with NOS3; furthermore, only the full-length isoform of CAPON can interact with NOS1 [54].

4.1 Nitric oxide signaling pathways

NO has been shown to signal through at least two distinct pathways: cGMP-dependent and cGMP-independent (S-nitrosylation) [55].

The cGMP-dependent effects result from the activation of guanylate cyclase, leading to increased cGMP levels, which modulate the activity of protein kinase G (PKG) or regulate the phosphodiesterases (PDE), with cGMP stimulating PDE2 and inhibiting PDE3. At low levels, NO can also directly activate adenylate cyclase, thus increasing cAMP levels and myocardial contractility [56].

On the other hand, cGMP-independent effects occur mainly via S-nitrosylation [57], a direct reaction between NO and thiol groups on cysteine residues causing changes in protein conformation. Additionally, NO may couple with other reactive oxygen and nitrogen species, leading to the formation of reactive chemical species, such as peroxynitrite ($ONOO^-$). Furthermore, NO-induced phosphorylation affects the function of proteins involved in excitation-contraction coupling (ECC).

4.2 Constitutive NOS activity and regulation of cardiac function

In the heart the functional role of NO is likely to depend largely on the spatial proximity of the target to the active NOS enzyme and the oxidative stress of the microenvironment. In cardiac myocytes, NOS3 is localized to the plasma membrane where it associate with caveolae [58, 59], whereas NOS1 is found close to the sarcoplasmic reticulum [50] where it is associated to ryanodine receptor Ca^{2+} release channel

(RyR). Therefore, differential spatial confinement of specific NOS isoforms is fundamental for the NOS1 and NOS3 independent, and in some cases opposite, effects on cardiac structure and function.

NOS1-derived NO has been shown to inhibit Ca^{2+} influx via the L-type Ca^{2+} channel (LTCC) [60], increase Ca^{2+} reuptake in the SR by increasing phospholamban (PLB) phosphorylation [61], and regulate the release of Ca^{2+} from SR through changes in RyR S-nitrosylation [62, 63]. NOS1 activity is in turn modulated by Ca^{2+} influx via the plasmalemmal Ca^{2+}-ATPase (PMCA) [64] (as the overexpression of PMCA4b inhibits NOS1 activity and blunts the β-adrenergic contractile response in cardiac myocytes [65]).

On the other hand, NOS3-derived NO has been reported to reduce myofilament Ca^{2+} sensitivity via PKG-mediated phosphorylation of troponin I [66], inhibit myocardial oxygen consumption [67, 68], and regulate intracellular cAMP levels (and thus, β-adrenergic responses) by modulating phosphodiesterases activity [69]. The stimulation of myocardial NOS3 activity by mechanical stretch has been shown to increase the open probability of the RyR channels [51]. Despite these and other studies, in vivo evidence that constitutively expressed NOS3 (in myocytes and endothelial cells) regulates cardiac function under basal conditions remains scant, and evidence from mice genetically lacking NOS3 suggests that any impact is minimal [70].

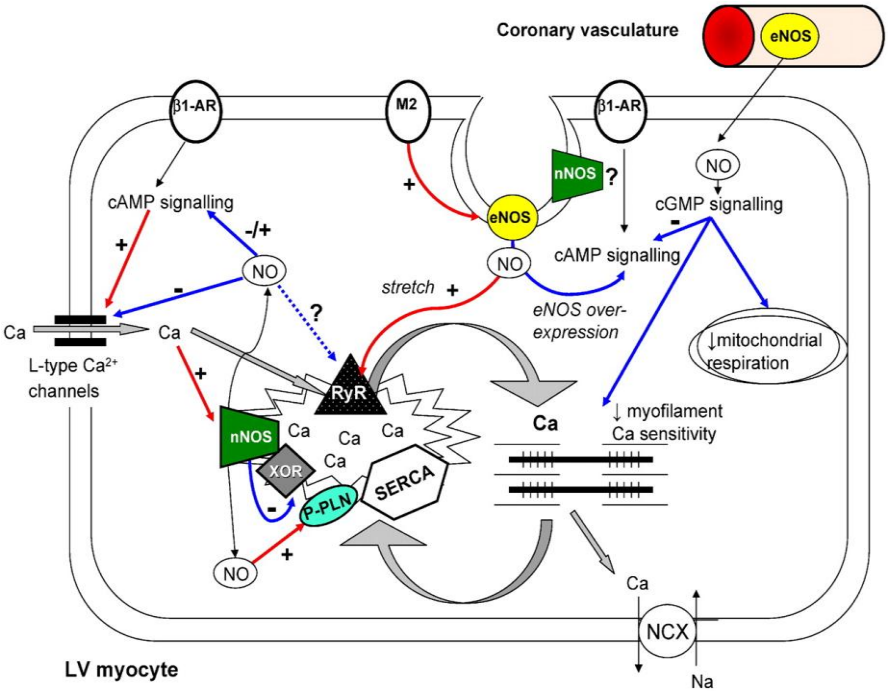

Figure 2. Regulation of myocardial Ca^{2+} fluxes by NOS-derived NO. From [71].

4.3 Evidence from NOS1-deletion models

NOS1 plays a key role in Ca^{2+} cycling acting as a major modulator of cardiac function and intracellular Ca^{2+} fluxes. Many investigators evaluated the effect of selective NOS1 gene deletion, both *in vivo* and in isolated cardiomyocytes. A summary of these effects are listed in **Table 3**. In particular, in $NOS1^{-/-}$ models, it has been reported an increased contractility [72-74], due to an increase in Ca^{2+} current density, Ca^{2+} transient amplitude and SR Ca^{2+} content [74]. NOS1 gene deletion has been reported to decrease RyR S-nitrosylation, but the impact of this finding on the RyR open probability remains a matter of debate. Gonzalez et al. reported an increase of diastolic Ca^{2+}

leak from the RyR in NOS1 knockout mice in the absence of differences in channel phosphorylation [75]; whereas Wang et al. [76] using the same model, reported a decrease in RyR open probability. Furthermore, NOS1 gene disruption also decreased PLB phosphorylation [77] due to enhanced protein phosphatases activity [61]. Finally, a further mechanism by which NOS1 can modulate ECC is through its interaction with xanthine oxidoreductase (XOR): in $NOS1^{-/-}$ mice model, XOR is activated and increases its production of superoxide, which, in turn, reduces myofilament Ca^{2+} sensitivity [78].

Many studies have focused the attention on NOS1 deletion effects in different cell models, but just few had investigated the consequence of CAPON modulation in cardiomyocytes (**Table 3**). Among them, Chang et al. overexpressed CAPON in guinea pig ventricular myocytes and they observed a shortening of the APD and a decrease in Ca^{2+} current density, changes compatible with reduced NOS1 activity [54]. More recently, Treuer et al. reported that CAPON silencing in cardiac myocytes using siRNA, significantly reduced the amplitude of electrically evoked Ca^{2+} transients and the degree of S-nitrosylation [79]. Taken together these results suggest that the function of NOS1 is closely related to CAPON activity/expression.

Preparation	Intervention	Effect
NOS1		
Sears et al. 2003 (Mouse)		
LV myocytes	NOS1 knockout or acute inhibition	↑ contraction ↑ I_{CaL} density ↑ SR load ↑ Ca^{2+} transient = diastolic Ca^{2+} = normal reuptake in SR
Khan et al. 2003 (Mouse)		
LV myocytes	NOS1 knockout	↓ force-frequency response (FFR) ↓ Ca^{2+} release ↑ SR Ca^{2+} stores ↑ SERCA2a ↓ PLB = NCX
Barouch et al. 2003 (Mouse)		
In vivo	NOS1 knockout	Cardiac hypertrophy ↑ mortality
Gonzalez et al. 2007 (Mouse)		
LV myocytes	NOS1 knockout	↓ sarcomere shortening ↓ Ca^{2+} transient diastolic Ca^{2+} leak and Ca^{2+} waves ↓ SR Ca^{2+} content ↓ RyR nitrosylation
Burkard et al. 2007 (Mouse)		
LV myocytes	NOS1 overexpression	NOS1 additionally localized at sarcolemma No association with RyR2 ↓ I_{CaL} density ↓ SR Ca^{2+} load ↓ Ca^{2+} transient ↓ PLB phosphorylation ↑ cGMP levels ↓ β-adrenergic response = LTCC, SERCA2a, NCX, PLB

Zhang et al. 2008 (Mouse)		
LV myocytes	NOS1 knockout	↓ PLB phosphorylation ↓RyR and troponin I PKA-dependent phosphorylation ↑ relaxation
Cutler et al. 2012 (Guinea Pig)		
Intact heart	NOS1 inhibition	Ca^{2+}-mediated triggered arrhythmias ↑ I_{CaL} density Frequent spontaneous Ca^{2+} transients and aftercontractions
CAPON		
Chang et al. 2007 (Guinea Pig)		
LV myocytes	CAPON overexpression	↓ APD (1, 2, 0.05 Hz) ↓ I_{CaL} density = I_{Na} and I_{K1} ↑ I_{Kr} density
Treuer, Gonzalez et al. 2014 (Rat)		
LV myocytes	CAPON Silencing	↓ Ca^{2+} transient ↓ S-nitrosylation

Table 3. Summary of the specific effects of NOS1 or CAPON modulation on basal and stimulated cardiac function taken from literature.

4.4 NOS activity in pathological conditions

Abnormal NOS function plays a key role in many cardiac disorders, partially because of defective NO signaling and partially because of excess production of oxygen radical species (oxidative stress). Indeed NOS produces a mixture of NO and superoxide species whose composition depends on cellular conditions, including availability of substrate (L-arginine) [80] and cofactors (tetrabiopterine, BH4). Reduced availability of such factors leads to NOS "uncoupling" and preferential synthesis of superoxide radicals over NO. Superoxide

radicals promote formation of reactive nitrogen (RNS) and oxygen (ROS) species which, in turn, can damage multiple cellular constituents, including membrane proteins and lipids. Furthermore, formation of RNS may reduce NO availability, therefore directly impairing its signaling. Although, when in limited amounts, radical species may act as physiological signals, their excess is implicated in the pathogenesis of many disorders. The impact of NOS-derived radicals is enhanced by scarce availability of radical scavenger molecules, as that occurring when further radical sources are activated by, for instance, hormones like angiotensin II [81]. The activity of NOS1 appears to be highly sensitive to changes in oxidative stress, which is typically increased by aging, ischemia [82] and pressure induced myocardial remodeling [83].

This sensitivity of NOS1 to cellular microenvironment is important as its activity is strictly confined, and for this reason its correct subcellular localization is crucial. Translocation and subsequent interaction with other target proteins or complexes could be important to differential modulation of cellular targets in physiological and pathological conditions. An up-regulation and translocation of NOS1 to mitochondria occurs in response to ischemia/reperfusion [84]. Similarly, NOS1 expression rises in human heart failure (HF) [85] and after myocardial infarction (MI) in rats, where translocation of the enzyme to the plasma membrane and its association with caveolin-3 is observed [86, 87]. Interestingly, in mice following MI, CAPON abundance is not altered, but the CAPON-NOS1 complex is relocalized to caveolar compartment of the plasma membrane [88]. Furthermore, in a mouse model of dystrophic cardiomyopathy that

presents arrhythmias, an increased expression of CAPON is observed, which is associated with dysfunction and altered Ca^{2+} cycling, as well as significant electrocardiogram abnormalities. The impact of this up-regulation remains to be determined, but may play a role in Ca^{2+} handling, NOS1 subcellular location and the arrhythmias presented in this model [89]. Taken together, all these observations, may be relevant to understand the importance of the correct subcellular localization of NOS1. In this setting, alteration in the expression of CAPON can be of particular relevance in altering the physiological activity of NOS1. Interestingly, CAPON mRNA levels are decreased in patients presenting the rs10494366 and rs10918594 NOS1AP polymorphisms [90], thus suggesting that the functional effect of these variants may results in a reduction of CAPON protein expression. Taking in account all the informations on CAPON and NOS1 function, this reduction may lead to abnormalities in NOS1 activity or localization and thus explain the association of NOS1AP SNPs with QT prolongation in the general population and increased incidence of SCD in LQTS patients.

5. Aim of the Thesis

Starting from the evidence that minor SNP variants of the NOS1AP gene have been reported to be associated with QT prolongation and increased incidence of sudden death in LQT1 patients, and the importance of CAPON protein in the activity of NOS1, we hypothesize that NOS1AP SNPs might affect NOS1 localization/function to decrease SR stability. As suggested by lack of a direct pathogenetic role of NOS1A SNPs, this effect would be clinically inconsequential under normal conditions. However, by affecting the Ca^{2+} influx/efflux balance, mutation-induced prolongation of repolarization may induce Ca^{2+} overload [3], whose proarrhythmic potential is expectedly enhanced by reduced SR stability. In other words, we propose that expressivity of LQTS mutations may require the coexistence of relative SR instability, as that potentially caused by specific NOS1AP variants.

My thesis work, presented in the enclose manuscript, tests this hypothesis by evaluating the effect of changes in NOS1 activity on SR functional stability, repolarization and arrhythmogenesis in the context of I_{Ks} deficiency, which simulates mutation-induced repolarization defect in LQT1 syndrome.

Bibliography

1. Schwartz, P.J. and M.J. Ackerman, *The long QT syndrome: a transatlantic clinical approach to diagnosis and therapy.* Eur Heart J, 2013. **34**(40): p. 3109-16.

2. Romano, C., G. Gemme, and R. Pongiglione, *[Rare Cardiac Arrythmias of the Pediatric Age. Ii. Syncopal Attacks Due to Paroxysmal Ventricular Fibrillation. (Presentation of 1st Case in Italian Pediatric Literature)]*. Clin Pediatr (Bologna), 1963. **45**: p. 656-83.

3. Schwartz, P.J., L. Crotti, and R. Insolia, *Long-QT syndrome: from genetics to management.* Circ Arrhythm Electrophysiol, 2012. **5**(4): p. 868-77.

4. Schwartz, P.J., et al., *Prevalence of the congenital long-QT syndrome.* Circulation, 2009. **120**(18): p. 1761-7.

5. Merri, M., et al., *Electrocardiographic quantitation of ventricular repolarization.* Circulation, 1989. **80**(5): p. 1301-8.

6. Priori, S.G., et al., *Risk stratification in the long-QT syndrome.* N Engl J Med, 2003. **348**(19): p. 1866-74.

7. Priori, S.G., C. Napolitano, and P.J. Schwartz, *Low penetrance in the long-QT syndrome: clinical impact.* Circulation, 1999. **99**(4): p. 529-33.

8. Schwartz, P.J., *The congenital long QT syndromes from genotype to phenotype: clinical implications.* J Intern Med, 2006. **259**(1): p. 39-47.

9. Crotti, L., et al., *Congenital long QT syndrome.* Orphanet J Rare Dis, 2008. **3**: p. 18.

10. Sanguinetti, M.C., *Long QT syndrome: ionic basis and arrhythmia mechanism in long QT syndrome type 1.* J Cardiovasc Electrophysiol, 2000. **11**(6): p. 710-2.

11. Jost, N., et al., *Restricting excessive cardiac action potential and QT prolongation: a vital role for IKs in human ventricular muscle.* Circulation, 2005. **112**(10): p. 1392-9.

12. Roden, D.M., *Long QT syndrome: reduced repolarization reserve and the genetic link.* J Intern Med, 2006. **259**(1): p. 59-69.

13. McDonald, T.F., et al., *Regulation and modulation of calcium channels in cardiac, skeletal, and smooth muscle cells.* Physiol Rev, 1994. **74**(2): p. 365-507.

14. Marx, S.O., et al., *Requirement of a macromolecular signaling complex for beta adrenergic receptor modulation of the KCNQ1-KCNE1 potassium channel.* Science, 2002. **295**(5554): p. 496-9.

15. Kenny, D. and R. Martin, *Drowning and sudden cardiac death.* Arch Dis Child, 2011. **96**(1): p. 5-8.

16. Roden DM. T*aking the idio out of idiosyncratic-predicting torsades de pointes*. Pacing Clin Electrophysiol, (1998). 21: 1029–1034.

17. Iost N, Virág L, Opincariu M, Szécsi J, Varró A, JGy P. *Does IKs play an important role in the repolarization in normal human ventricular muscle?* Circulation (1999). 100(1): I–495.

18. Varró A, Baláti B, Iost N, Takács J, Virág L, Lathrop DA et al., *The role of IKs in dog ventricular muscle and Purkinje fibre repolarization*. J Physiol, 2000. 523: 67–81.

19. Lengyel C, Iost N, Virág L, Varró A, Lathrop DA, Papp JG *Pharmacological block of the slow component of the outward delayed rectifier current (IKs) fails to lengthen rabbit ventricular muscle QTc and action potential duration*. Br J Pharmacol, 2001. 132:101–110.

20. Jost N, Virág L, Bitay M, Takács J, Lengyel C, Biliczki P et al., *Restricting excessive cardiac action potential and QT prolongation: a vital role for IKs in human ventricular muscle*. Circulation, 2005.112: p. 1392–1399.

21. Roden DM. *Long QT syndrome: reduced repolarization reserve and the genetic link*. J Intern Med, 2006. 259: p. 59–69.

22. Zaniboni M, Pollard AE, Yang L, Spitzer KW, *Beat-to-beat repolarization variability in ventricular myocytes and its suppression by electrical coupling.* Am J Physiol Heart Circ Physiol, 2000. 278: p. H677–687.

23. Hinterseer M, Beckmann BM, Thomsen MB, Pfeufer A, Ulbrich M, et al., *Usefulness of short-term variability of QT intervals as a predictor for electrical remodeling and proarrhythmia in patients with nonischemic heart failure.* Am J Cardiol, 2010. 106: p. 216–220.

24. Tereshchenko LG, Han L, Cheng A, Marine JE, Spragg DD, et al., *Beat-to-beat three-dimensional ECG variability predicts ventricular arrhythmia in ICD recipients*. Heart Rhythm, 2010. 7: p. 1606–1613.

25. Thomsen MB, Verduyn SC, Stengl M, Beekman JD, de Pater G, et al., *Increased short-term variability of repolarization predicts d-sotalol-induced torsades de pointes in dogs*. Circulation, 2004. 110: p. 2453–2459.

26. Gallacher DJ, Van de Water A, van der Linde H, Hermans AN, Lu HR, et al., *In vivo mechanisms precipitating torsades de pointes in a canine model of drug-induced long-QT1 syndrome*. Cardiovasc Res, 2007. 76: p. 247–256.

27. Jacobson I, Carlsson L, Duker G, *Beat-by-beat QT interval variability, but not QT prolongation per se, predicts drug-induced torsades de pointes in the anaesthetised methoxamine-sensitized rabbit*. J Pharmacol Toxicol Methods, 2011. 63: p. 40–46.

28. Hinterseer M, Beckmann BM, Thomsen MB, Pfeufer A, Dalla Pozza R, et al., *Relation of increased short-term variability of*

QT interval to congenital long-QT syndrome. Am J Cardiol 2009. 103: p. 1244–1248.

29. Bilchick K, Viitasalo M, Oikarinen L, Fetics B, Tomaselli G, Swan H, Laitinen PJ, Vaananen H, Kontula K, Berger RD. *Temporal repolarization lability differences among genotyped patients with the long QT syndrome*. Am J Cardiol. 2004. 94:p. 1312–1316.

30. Perkiomaki JS, Zareba W, Nomura A, Andrews M, Kaufman ES, Moss AJ. *Repolarization dynamics in patients with long QT syndrome*. J Cardiovasc Electrophysiol. 2002. 13: p. 651–656.

31. Haigney MC, Zareba W, Gentlesk PJ, Goldstein RE, Illovsky M, McNitt S, Andrews ML, Moss AJ. *QT interval variability and spontaneous ventricular tachycardia or fibrillation in the multicenter automatic defibrillator implantation trial (MADIT) II patients*. J Am Coll Cardiol. 2004. 44: p. 1481–1487.

32. Segerson NM, Litwin SE, Daccarett M, Wall TS, Hamdan MH, Lux RL. *Scatter in repolarization timing predicts clinical events in post-myocardial infarction patients*. Heart Rhythm. 2008. 5: p. 208–214.

33. Szentandrássy N, Kistamás K, Hegyi B, Horváth B, Ruzsnavszky F, Váczi K, et al. *Contribution of ion currents to beat-to-beat variability of action potential duration in canine ventricular myocytes*. Pflugers Arch. 2015; 467(7):1431–43.

34. Johnson DM, Heijman J, Bode EF, Greensmith DJ, van der Linde H, Abi-Gerges N, et al. *Diastolic spontaneous calcium release from the sarcoplasmic reticulum increases beat-to-beat variability of repolarization in canine ventricular myocytes after β-adrenergic stimulation*. Circ Res, 2013; 112, p. 246–256.

35. Wilke, R.A., et al., *Identifying genetic risk factors for serious adverse drug reactions: current progress and challenges.* Nat Rev Drug Discov, 2007. **6**(11): p. 904-16.

36. Napolitano, C., et al., *Genetic modulators of the phenotype in the long QT syndrome: state of the art and clinical impact.* Curr Opin Genet Dev, 2015. **33**: p. 17-24.

37. Sotoodehnia, N., et al., *Common variants in 22 loci are associated with QRS duration and cardiac ventricular conduction.* Nat Genet, 2010. **42**(12): p. 1068-76.

38. Tomas, M., et al., *Polymorphisms in the NOS1AP gene modulate QT interval duration and risk of arrhythmias in the long QT syndrome.* J Am Coll Cardiol, 2010. **55**(24): p. 2745-52.

39. Earle, N., et al., *Single nucleotide polymorphisms in arrhythmia genes modify the risk of cardiac events and sudden death in long QT syndrome.* Heart Rhythm, 2014. **11**(1): p. 76-82.

40. Wratten, N.S., et al., *Identification of a schizophrenia-associated functional noncoding variant in NOS1AP*. Am J Psychiatry, 2009. **166**(4): p. 434-41.

41. Eijgelsheim M, Aarnoudse AL, Rivadeneira F, et al., *Identification of a common variant at the NOS1AP locus strongly associated to QT-interval duration.*. Hum Mol Genet, 2009. **18**: p. 347-57.

42. JPost W., Shen H., Damcott C., Arking D.E., Kao W.H., Sack P.A., Ryan K.A., Chakravarti A., Mitchell B.D., Shuldiner A.R. *Associations between genetic variants in the NOS1AP (CAPON) gene and cardiac repolarization in the old order Amish. Hum. Hered. 2007;64:214-219.*

43. Aarnoudse A.J., Newton-Cheh C., de Bakker P.I., Straus S.M., Kors J.A., Hofman A., Uitterlinden A.G., Witteman J.C., Stricker B.H.*Common NOS1AP variants are associated with a prolonged QTc interval in the Rotterdam Study. Circulation 2007;116:10-16.*

44. Arking D.E., Pfeufer A., Post W., Kao W.H., Newton-Cheh C., Ikeda M., West K., Kashuk C., Akyol M., Perz S., et al. *A common genetic variant in the NOS1 regulator NOS1AP modulates cardiac repolarization. Nat. Genet. 2006;38:644-651.*

45. Jaffrey, S.R., et al., *CAPON: a protein associated with neuronal nitric oxide synthase that regulates its interactions with PSD95.* Neuron, 1998. **20**(1): p. 115-24.

46. Xu, B., et al., *Increased expression in dorsolateral prefrontal cortex of CAPON in schizophrenia and bipolar disorder.* PLoS Med, 2005. **2**(10): p. e263.

47. Fang, M., et al., *Dexras1: a G protein specifically coupled to neuronal nitric oxide synthase via CAPON.* Neuron, 2000. **28**(1): p. 183-93.

48. Barouch, L.A., et al., *Nitric oxide regulates the heart by spatial confinement of nitric oxide synthase isoforms.* Nature, 2002. **416**(6878): p. 337-9.

49. Ziolo, M.T. and D.M. Bers, *The real estate of NOS signaling: location, location, location.* Circ Res, 2003. **92**(12): p. 1279-81.

50. Xu, K.Y., et al., *Nitric oxide synthase in cardiac sarcoplasmic reticulum.* Proc Natl Acad Sci U S A, 1999. **96**(2): p. 657-62.

51. Petroff, M.G., et al., *Endogenous nitric oxide mechanisms mediate the stretch dependence of Ca2+ release in cardiomyocytes.* Nat Cell Biol, 2001. **3**(10): p. 867-73.

52. Nishida, C.R. and P.R. Ortiz de Montellano, *Electron transfer and catalytic activity of nitric oxide synthases. Chimeric*

constructs of the neuronal, inducible, and endothelial isoforms. J Biol Chem, 1998. **273**(10): p. 5566-71.

53. Ziolo, M.T., et al., *Myocytes isolated from rejecting transplanted rat hearts exhibit a nitric oxide-mediated reduction in the calcium current.* J Mol Cell Cardiol, 2001. **33**(9): p. 1691-9.

54. Chang, K.C., et al., *CAPON modulates cardiac repolarization via neuronal nitric oxide synthase signaling in the heart.* Proc Natl Acad Sci U S A, 2008. **105**(11): p. 4477-82.

55. Ziolo, M.T., *The fork in the nitric oxide road: cyclic GMP or nitrosylation?* Nitric Oxide, 2008. **18**(3): p. 153-6.

56. Vila-Petroff, M.G., et al., *Activation of distinct cAMP-dependent and cGMP-dependent pathways by nitric oxide in cardiac myocytes.* Circ Res, 1999. **84**(9): p. 1020-31.

57. Stamler, J.S., S. Lamas, and F.C. Fang, *Nitrosylation. the prototypic redox-based signaling mechanism.* Cell, 2001. **106**(6): p. 675-83.

58. Balligand, J.L., et al., *Nitric oxide-dependent parasympathetic signaling is due to activation of constitutive endothelial (type III) nitric oxide synthase in cardiac myocytes.* J Biol Chem, 1995. **270**(24): p. 14582-6.

59. Feron, O., et al., *Endothelial nitric oxide synthase targeting to caveolae. Specific interactions with caveolin isoforms in*

cardiac myocytes and endothelial cells. J Biol Chem, 1996. **271**(37): p. 22810-4.

60. Burkard, N., et al., *Conditional neuronal nitric oxide synthase overexpression impairs myocardial contractility.* Circ Res, 2007. **100**(3): p. e32-44.

61. Zhang, Y.H., et al., *Reduced phospholamban phosphorylation is associated with impaired relaxation in left ventricular myocytes from neuronal NO synthase-deficient mice.* Circ Res, 2008. **102**(2): p. 242-9.

62. Zahradnikova, A., et al., *Inactivation of the cardiac ryanodine receptor calcium release channel by nitric oxide.* Cell Calcium, 1997. **22**(6): p. 447-54.

63. Xu, L., et al., *Activation of the cardiac calcium release channel (ryanodine receptor) by poly-S-nitrosylation.* Science, 1998. **279**(5348): p. 234-7.

64. Schuh, K., et al., *The plasmamembrane calmodulin-dependent calcium pump: a major regulator of nitric oxide synthase I.* J Cell Biol, 2001. **155**(2): p. 201-5.

65. Oceandy, D., et al., *Neuronal nitric oxide synthase signaling in the heart is regulated by the sarcolemmal calcium pump 4b.* Circulation, 2007. **115**(4): p. 483-92.

66. Layland, J., J.M. Li, and A.M. Shah, *Role of cyclic GMP-dependent protein kinase in the contractile response to*

exogenous nitric oxide in rat cardiac myocytes. J Physiol, 2002. **540**(Pt 2): p. 457-67.

67. Loke, K.E., et al., *Endogenous endothelial nitric oxide synthase-derived nitric oxide is a physiological regulator of myocardial oxygen consumption.* Circ Res, 1999. **84**(7): p. 840-5.

68. Xie, Y.W. and M.S. Wolin, *Role of nitric oxide and its interaction with superoxide in the suppression of cardiac muscle mitochondrial respiration. Involvement in response to hypoxia/reoxygenation.* Circulation, 1996. **94**(10): p. 2580-6.

69. Godecke, A., et al., *Inotropic response to beta-adrenergic receptor stimulation and anti-adrenergic effect of ACh in endothelial NO synthase-deficient mouse hearts.* J Physiol, 2001. **532**(Pt 1): p. 195-204.

70. Kondo, K., et al., *H(2)S protects against pressure overload-induced heart failure via upregulation of endothelial nitric oxide synthase.* Circulation, 2013. **127**(10): p. 1116-27.

71. Mike Seddon, Ajay M. Shah, Barbara Casadei, *Cardiomyocytes as effectors of nitric oxide signalling*. Cardiovascular Research, 2007. 75(2): p. 315-326.

72. Burger, D.E., et al., *Neuronal nitric oxide synthase protects against myocardial infarction-induced ventricular arrhythmia and mortality in mice.* Circulation, 2009. **120**(14): p. 1345-54.

73. Dawson, D., et al., *nNOS gene deletion exacerbates pathological left ventricular remodeling and functional deterioration after myocardial infarction.* Circulation, 2005. **112**(24): p. 3729-37.

74. Sears, C.E., et al., *Cardiac neuronal nitric oxide synthase isoform regulates myocardial contraction and calcium handling.* Circ Res, 2003. **92**(5): p. e52-9.

75. Gonzalez, D.R., et al., *Deficient ryanodine receptor S-nitrosylation increases sarcoplasmic reticulum calcium leak and arrhythmogenesis in cardiomyocytes.* Proc Natl Acad Sci U S A, 2007. **104**(51): p. 20612-7.

76. Wang H, Viatchenko-Karpinski S, Sun J, Györke I, Benkusky NA, Kohr MJ, Valdivia HH, Murphy E, Györke S, Ziolo MT et al., *Regulation of myocyte contraction via neuronal nitric oxide synthase: role of ryanodine receptor S-nitrosylation.* J Physiol, 2010. **1** (588): p. 2905-17.

77. Wang, H., et al., *Neuronal nitric oxide synthase signaling within cardiac myocytes targets phospholamban.* Am J Physiol Cell Physiol, 2008. **294**(6): p. C1566-75.

78. Khan, S.A., et al., *Neuronal nitric oxide synthase negatively regulates xanthine oxidoreductase inhibition of cardiac excitation-contraction coupling.* Proc Natl Acad Sci U S A, 2004. **101**(45): p. 15944-8.

79. Treuer, A.V., Gonzalez D.R, *NOS1AP modulates intracellular Ca2+ in cardiac myocytes and is up-regulated in dystrophic cardiomyopathy.*, Int J Physiol Pathophysiol Pharmacol, 2014. **6**(1): p. 37-46.

80. Dudzinski, D.M., et al., *The regulation and pharmacology of endothelial nitric oxide synthase.* Annu Rev Pharmacol Toxicol, 2006. **46**: p. 235-76.

81. Swedberg, K., et al., *Hormones regulating cardiovascular function in patients with severe congestive heart failure and their relation to mortality. CONSENSUS Trial Study Group.* Circulation, 1990. **82**(5): p. 1730-6.

82. Ferrari, R., et al., *Oxidative stress during myocardial ischaemia and heart failure.* Eur Heart J, 1998. **19 Suppl B**: p. B2-11.

83. Piech, A., et al., *Differential regulation of nitric oxide synthases and their allosteric regulators in heart and vessels of hypertensive rats.* Cardiovasc Res, 2003. **57**(2): p. 456-67.

84. Burkard, N., et al., *Conditional overexpression of neuronal nitric oxide synthase is cardioprotective in ischemia/reperfusion.* Circulation, 2010. **122**(16): p. 1588-603.

85. Damy, T., et al., *Increased neuronal nitric oxide synthase-derived NO production in the failing human heart.* Lancet, 2004. **363**(9418): p. 1365-7.

86. Bendall, J.K., et al., *Role of myocardial neuronal nitric oxide synthase-derived nitric oxide in beta-adrenergic hyporesponsiveness after myocardial infarction-induced heart failure in rat.* Circulation, 2004. **110**(16): p. 2368-75.

87. Damy, T., et al., *Up-regulation of cardiac nitric oxide synthase 1-derived nitric oxide after myocardial infarction in senescent rats.* FASEB J, 2003. **17**(13): p. 1934-6.

88. Beigi F, Oskouei BN, Zheng M, Cooke CA, Lamirault G, Hare JM., *Cardiac nitric oxide synthase-1 localization within the cardiomyocyte is accompanied by the adaptor protein, CAPON*. Nitric Oxide, 2009. **21**(3-4): p. 226-33.

89. Bia BL, Cassidy PJ, Young ME, Rafael JA, Leighton B, Davies KE, Radda GK, Clarke K**.,** *Decreased myocardial nNOS, increased iNOS and abnormal ECGs in mouse models of Duchenne muscular dystrophy*. J Mol Cell Cardiol. 1999. **31**(10): p. 1857-62.

90. S. Saba *et al., Cardiac levels of NOS1AP RNA from right ventricular tissue recovered during lead extraction*. Heart Rhythm, 2012. **9**(3): p. 399–404.

Chapter 2

Modifier genes in the LQT1 syndrome, mechanistic analysis of NOS1AP polymorphism.

Joyce Bernardi, MS[1]; Carlotta Ronchi, PhD[1]; Eleonora Torre, MS[1]; Gaspare Mostacciuolo, Mr[1]; Marcella Rocchetti, PhD[1]; Antonio Zaza, MD[1].

[1] Department of Biotechnologies and Biosciences, University of Milano-Bicocca, Milan, Italy.

Acronyms

AP	action potential
APD	action potential duration
APD_{90}	action potential duration at 90% of repolarization
Ca_D	diastolic Ca^{2+}
Ca_T	Ca^{2+} transient amplitude
CTRL	control
CM	cardiomyocyte
DADs	delayed afterdepolarizations
E_{rev}	reversal potential
G_{max}	maximal conductance
I_{CaL}	L-type Ca^{2+} current
I_{Kr}	rapidly activating delayed rectifier potassium channels
I_{Ks}	slowly activating delayed rectifier potassium channels
iPSC-CMs	induced pluripotent stem cell-derived cardiomyocytes
ISO	isoproterenol
I_{TI}	transient inward current
L-VNIO	vynil-L-NIO [N^5-(1-imino-3-butenyl)-L-ornithine]
LQT1	long QT syndrome type 1
NOS1	nitric oxide synthase
NOS1AP	nitric oxide synthase adaptor protein 1
SMTC	S-methyl-L-thiocitrulline
SR	sarcoplasmic reticulum

1. Introduction

LQT1 is a genetic disorder characterized by a pathological prolongation of the QT interval in ECG, and is caused by mutations of the KCNQ1 gene, that lead to a loss of function of the repolarizing current I_{Ks} [1]. This is associated with repolarization delay and a high risk of life threatening arrhythmias during sympathetic activation. However, carriers of the same LQT1 mutation may be strongly symptomatic at young age, or asymptomatic through their whole life, sometimes even failing to show QT prolongation. In this setting, genotyping may be inadequate to predict the risk of sudden death, a major difficulty in the clinical management of LQT patients. This phenotypic variability suggests the existence of factors, beyond the primary mutation, that can modify mutation expressivity. Identification of genetic modifiers of LQTS would lead to improved risk stratification of mutation carriers; furthermore, demonstration of a causative role of the modifier and clarification of the underlying mechanisms may lead to the identification of novel therapeutic targets. Recently, minor SNP variants of the NOS1AP gene have been reported to be associated with QT prolongation and increased incidence of sudden death in LQT1 patients [2, 3]. NOS1AP variants are located in noncoding regions of the gene; therefore, the role of these SNPs is likely at the level of transcriptional regulation [4-6]. The NOS1AP gene encodes for CAPON protein, that localizes NOS1 close to the sarcoplasmic reticulum (SR) [7]. NOS1 activity is important for NO-mediated modulation of I_{CaL}[8, 9], RyR2 channels [10-12] and

SERCA [13, 14], thus interfering with regulation of Ca^{2+} handling and SR stability.

In 2008 Chang et al. overexpressed CAPON in guinea-pig ventricular myocytes and they observed a shortening of the APD and a decrease in Ca^{2+} current density, changes compatible with reduced NOS1 activity [15]. This suggests that the function of NOS1 is closely related to CAPON activity/expression.

We hypothesize that NOS1AP SNPs might affect NOS1 localization/function to decrease SR stability. In this setting, mutation-induced QT prolongation would induce Ca^{2+} overload, whose proarrhythmic effect would be unveiled by abnormal NOS1 localization/function.

The aim of this research was to evaluate the effect of changes in NOS1 activity on SR functional stability, repolarization and arrhythmogenesis in the context of I_{Ks} deficiency (simulating LQT1).

2. Methods

2.1 Cell Isolation

Dunkin-Hartley guinea pigs were euthanized by cervical dislocation under 800 mg/Kg chloral hydrate intraperitoneally anesthesia. Ventricular myocytes were isolated by using a retrograde coronary perfusion method previously published [16], with minor modifications. Rod-shaped, Ca^{2+}-tolerant myocytes were used within 12 h from dissociation. All experiments conformed to the guidelines for Animal Care endorsed by the University of Milano-Bicocca.

2.2 Experimental model

To reproduce the LQT1 phenotype we subjected guinea pig ventricular myocytes to I_{Ks} blockade (2µM JNJ303) and adrenergic stimulation (isoproterenol, ISO 1 nM). In this cells we measured electrical activity, membrane currents and intracellular Ca^{2+} dynamics, in basal condition (CTRL group) and under selective inhibition of NOS1 activity by incubation with 3µM S-methyl-L-thiocitrulline (SMTC) for at least 30 minutes (SMTC group). As a confirmation, for some experiments we also used another NOS1 specific inhibitor, vynil-L-NIO (L-VNIO) 100 µM. NOS1 inhibitors were added both in the perfusion solution and dialyzed into the cell through the patch pipette.

2.3 Patch-clamp recording

All measurements were performed in the whole-cell configuration on freshly isolated guinea pig ventricular myocytes at physiological temperature (36°C). Recordings were carried out under superfusion with standard Tyrode's solution containing (mM): 154 NaCl, 4 KCl, 2 $CaCl_2$, 1 $MgCl_2$, 5 HEPES-NaOH, 5.5 D-glucose, adjusted to pH 7.35 with NaOH. Membrane capacitance and series resistance were measured in every cells. Signals were acquired with a MultiClamp 700B amplifier (Axon Instrument), connected to a Digidata 1440A (Molecular Devices) and filtered with an appropriate Bessel filter via pClamp 10 (Molecular Devices).

2.4 Action potential measurements

Action potentials (APs) were recorded in current-clamp mode during steady-state pacing at a cycle length of 2 Hz. Action potential duration at 90% repolarization (APD_{90}) was measured by automatic computer routines. The incidence and time of occurrence of delayed afterdepolarizations (DADs), reflecting the occurrence of intracellular Ca^{2+} waves, was measured. DADs were defined as transient membrane depolarizations >0.5 mV occurring after AP repolarization [17].

2.5 AP-clamp experiments

This set of experiments aimed to test the role of prolonged APD in generating SR instability under control conditions and NOS1 inhibition. APs whose duration differed by a proportion roughly representative of QT prolongation in LQT1 patients (short AP: APD_{90} = 100 ms, long AP: APD_{90} = 140 ms; corresponding to 40% QTc prolongation) were recorded at 2 Hz under I-clamp conditions; the respective waveforms were used as "command potential" to drive membrane potential in action potential clamp (AP-clamp) experiments. In the latter, total membrane current was recorded during repetitive application of AP waveforms at 2 Hz. Inward current transients (I_{TI}) occurring after repolarization were assumed to reflect the occurrence of intracellular Ca^{2+} waves, a sign of SR instability. I_{TI} incidence were compared between short and long APs respectively.

2.6 I_{CaL} measurements

I_{CaL} was isolated by using a Na^+- and K^+-free extracellular solution containing (mM): 154 tetraethylammonium chloride (TEACl), 1 $MgCl_2$, 2 $CaCl_2$, 5 HEPES, 5.5 D-glucose, with pH adjusted to 7.4 with TEAOH. Intracellular solution contained (mM): 115 CsCl, 20 TEACl, 0.5 $MgCl_2$, 10 EGTA CsOH, 5 HEPES CsOH, 5 ATP Mg^{2+}-salt, 5 creatine phosphate Tris-salt, 0.4 GTP Tris-salt; at pH 7.2 with CsOH. I_{CaL} was elicited by a 300 ms V steps from -50 to +60 mV from an holding potential of -40 mV. Activation and inactivation curves were obtained from peak current I/V relationship as previously described [18] and fitted with Boltzmann functions to extract gating parameters, including voltage of half-maximal activation/inactivation ($V_{0.5}$, mV), slope factor (k, mV), and maximal conductance (g_{max}, nS). Series resistance was compensated to minimize voltage error.

2.7 I_{Ks} and I_{Kr} measurements

I_{Ks} and I_{Kr} were isolated by subtraction, as currents sensitive to their specific blockers JNJ303 (2 µM) and E4031 (5 µM) respectively. Pipette solution contained (mM): 110 K^+-aspartate, 23 KCl, 3 $MgCl_2$, 2 $CaCl_2$, 5 HEPES-KOH, 5 EGTA-KOH, 5 ATP Na^+-salt, 5 creatine phosphate Na^+-salt, 0.4 GTP Na^+-salt, pH adjusted to 7.3 with KOH.
5 µM nifedipine was added to rule out interference by I_{CaL}. From a holding potential of -40 mV for both currents, 10 depolarizing steps of 5s (with 10 mV increments) were applied at a CL of 11 s for I_{Ks} measurement, while I_{Kr} was elicited by a 1 s voltage steps with an

interpulse interval of 3 s. Current was measured as peak current occurring upon repolarization to holding potential (tail current amplitude) for both currents.

2.8 Intracellular Ca^{2+} measurements

Cytosolic Ca^{2+} dynamics was recorded in myocytes loaded with 10 µM Fluo4-AM and stimulated under I-clamp at 2 Hz. Fluo4 was excited at a wavelength of 494 nm and emission was collected through a 535 nm band pass filter. Light emission was amplified, converted to voltage, low-pass filtered (200 Hz) and digitized at 2 kHz. If necessary, further low-pass digital filtering (FFT, 100 Hz) was applied during analysis. Ca^{2+} signal was evaluated in terms of Ca^{2+} transient amplitude (Ca_T) and diastolic Ca^{2+} (Ca_D). Fluorescence signal recorded in basal condition before ISO application was used, after subtraction of background luminescence, as reference fluorescence (F_0) for signal normalization (F/F_0).

2.9 Statistical analysis

Student's paired or unpaired t-test were applied as appropriate to test for significance between means. Difference between categorical variables was tested by chi^2 analysis. Average data are expressed and plotted as mean ± standard error of the mean. Statistical significance was defined as $P<0.05$ (NS, not significant). Sample size (n, number of cells) is specified for each experimental condition in the respective figure legend.

3. Results

3.1 Effect of NOS1 inhibition on Action Potential

This set of experiments aimed at testing the effect of NOS1 inhibition on repolarization under conditions simulating the arrhythmogenic setting of LQT1 (I_{Ks} blockade and β-adrenergic activation).

To this end we compared APD_{90} between control (CTRL) and NOS1 blockade by SMTC. Under basal conditions, mean APD_{90} was significantly prolonged after NOS1 inhibition (152.6 ± 11.7 ms; n=15) compared to CTRL (96.1 ± 9.0 ms; n=27. $P<0.01$) (**Figure 1.** A); NOS1 blockade prolonged APD_{90} by 58.8 %.

To reproduce the LQT1 phenotype, I_{Ks} was blocked in CTRL and SMTC treated myocytes. I_{Ks} blockade prolonged APD_{90} to a comparable extent between the two groups (10.6 ± 2.7 % in SMTC vs 10.8 ± 2.0 % in CTRL, NS), thus suggesting that NOS1 inhibition did not interfere with I_{Ks} channel activity.

β-adrenergic stimulation by isoproterenol (ISO 1 nM) was then superimposed on I_{Ks} blockade. ISO further prolonged APD_{90}, and this prolongation was significantly larger in SMTC myocytes (39.7 ± 5.1 %) than in CTRL ones (24.2 ± 4.0 %, $P<0.03$).

To summarize, NOS1 inhibition significantly prolonged APD_{90} under basal condition, did not change the effect of I_{Ks} blockade, but almost doubled the prolonging effect of superimposed ISO.

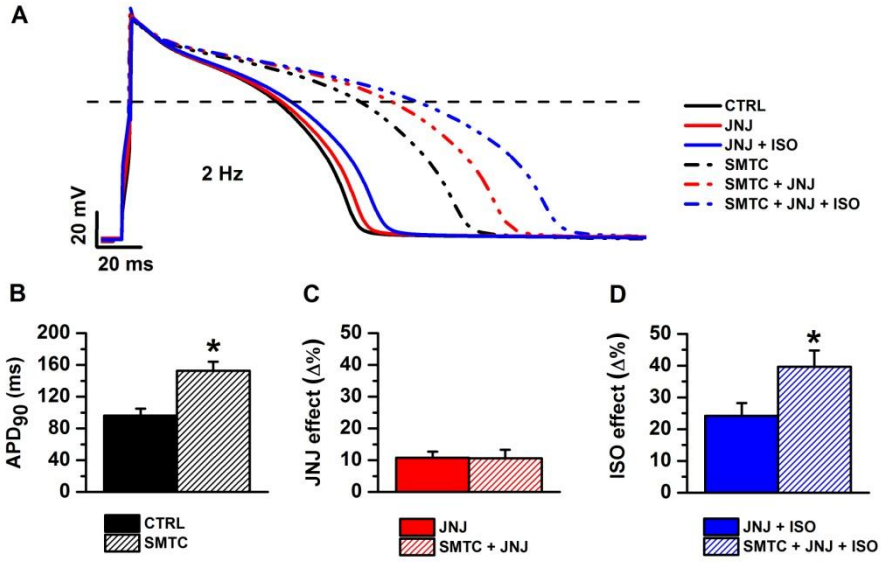

Figure 1. A) Representative APs from CTRL and SMTC cells stimulated at 2 Hz, in basal condition (black), after I_{Ks} blockade with 2 µM JNJ303 alone (red) or with 1 nM of ISO (blue). B) Analysis of APD_{90} in basal condition. Effect (Δ%) of I_{Ks} blockade alone (C) and with ISO (D) in the two groups. (CTRL n=27, SMTC n=15). *= P<0.05 vs CTRL.

3.2 Effect of NOS1 inhibition on DADs occurrence

DADs, absent under baseline conditions, often occurred when ISO was applied to myocytes in which I_{Ks} had been blocked. ISO induced DADs in 14 of 15 SMTC-treated myocytes, as compared to 6 of 27 CTRL myocytes (93% vs 22% ; P<0.01. **Figure 2.** A). Moreover, we analyzed the time at which DADs arose after starting ISO superfusion. The average time of DADs appearance was significantly shorter in SMTC treated myocytes than in CTRL ones (25.8 ± 3.8 s vs 61.5 ± 15.3 s, P<0.01; **Figure 2.** B).

To rule out that the observations resulted from SMTC effect other than NOS1 inhibition (ancillary effects), experiments were repeated using a different NOS1-specific inhibitor, L-VNIO (100 μM). In these experiments two concentration of ISO (1 and 10 nM) were also tested. The lower ISO concentration induced DADs in 6 of 9 (L-VNIO treated myocytes and none of 11 CTRL myocytes (66.7% vs 0%; $P<0.01$. **Figure 2.** C). At the higher ISO concentration DADs occurred in 100% of both CTRL and L-VNIO treated myocytes (**Figure 2.** D); however, the time of DADs occurrence was significantly shorter in L-VNIO treated than in CTRL myocytes (14.7 ± 2.4 s vs 35.6 ± 7.2 s, $P<0.03$; **Figure 2.** E). In particular, at this ISO concentration, only in L-VNIO treated myocytes DADs occasionally (4 of 9 cells) resulted in triggered activity ($P<0.01$ vs CTRL. **Figure 2.** F and G).

To summarize, NOS1 inhibition (by two unrelated compounds), strongly facilitated DADs induction by β-adrenergic stimulation on a background of I_{Ks} deficiency.

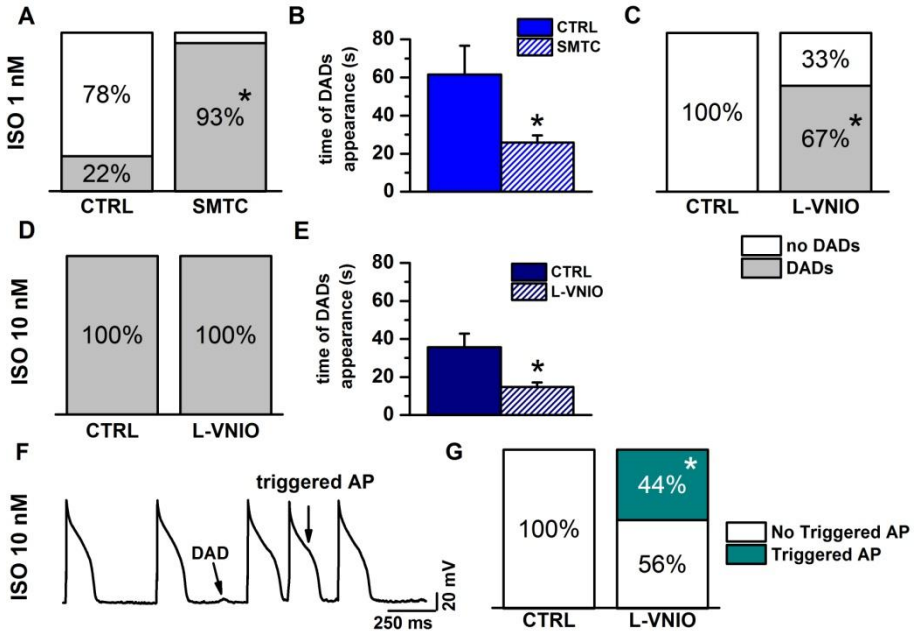

Figure 2. Percentage (A) and different time (B) of DADs appearance in CTRL and SMTC treated cells after superfusion with 1 nM ISO (CTRL n=27, SMTC n=15). C) Different incidence of DADs appearance following 1 nM (C) and 10 nM (D) ISO superfusion, in CTRL myocytes or after incubation with L-VNIO (100 µM). E) Time of DADs appearance after 10 nM ISO application in CTRL and L-VNIO myocytes. F) Example of delayed afterdepolarizations (DADs) and DAD-induced triggered AP appearance, and G) analysis of triggered activity incidence between CTRL and L-VNIO myocytes after 10 nM ISO application (CTRL n=11, L-VNIO n=9). *=P<0.05 vs CTRL.

3.3 Effect of NOS1 inhibition on repolarizing currents

The aim of these experiments was to test the effect of NOS1 inhibition on the membrane currents more likely to account for its effect on repolarization (above). These include the high-threshold Ca^{2+} current (I_{CaL}) and delayed rectifier K^+ currents (I_{Kr} and I_{Ks}).

I_{CaL} is, at the same time, the main contributor of inward current during repolarization, the trigger of Ca^{2+} release from the SR (peak component) and the route of sarcolemmal Ca^{2+} influx (peak + window components). "Delayed rectifier" K^+ current is the main outward component contributing to repolarization velocity, it consists of two components: rapidly activating (I_{Kr}) and slowly activating (I_{Ks}) [19]. Abnormalities in either I_{Kr} or I_{Ks} occur in LQTS and are associated with prolongation and instability of repolarization.

3.3.1 *High threshold Ca^{2+} current (I_{CaL})*

Peak I_{CaL} density was significantly enhanced in SMTC treated myocytes (-16.6 ± 1.2 pA/pF, at +10 mV, n=20) compared to CTRL ones (-13.5 ± 1.0 pA/pF, at +10 mV, n=25; $P<0.05$) (**Figure 3.** B and D). SMTC-induced enhancement of peak I_{CaL} density amounted to 24 %. We further investigated whether SMTC-induced I_{CaL} enhancement was due to changes in the fully-activated properties conductance (E_{rev}, g_{max}) or in the voltage-dependency of steady-state channel activation or inactivation.

I_{CaL} reversal potential (E_{rev}) was similar between SMTC treated and CTRL myocytes (62.2 ± 1.0 mV vs 60.3 ± 0.9 mV, NS).

Maximal I_{CaL} conductance (g_{max}, normalized to capacitance) was significantly larger in SMTC treated myocytes than in CTRL ones (0.35 ± 0.02 nS/pF, n=20 vs 0.29 ± 0.02 nS/pF, n=25; $P<0.05$). I_{CaL} mean activation curve was superimposable between CTRL and SMTC treated myocytes; inactivation was slightly shifted positive in SMTC treated myocytes but this was not reflected by a difference in gating parameters (**Figure 3**. C). Activation $V_{0.5}$ was unchanged by SMTC (-3.9 ± 0.7 mV vs -3.6 ± 0.5 mV, NS), the same was true for the activation slope factor (6.9 ± 0.1 mV vs 7.0 ± 0.1 mV, NS). Inactivation parameters, which could be safely analyzed only in a subset of cells (SMTC n=17, CTRL n=13), were also comparable between SMTC treated and CTRL myocytes. Inactivation $V_{0.5}$ was -22.1 ± 0.6 mV vs -23.8 ± 1.0 mV and the slope factor was 4.4 ± 0.2 mV vs 4.8 ± 0.5 mV for SMTC treated and CTRL myocytes respectively.

Taken together these results indicate that the effect of NOS1 inhibition on peak I_{CaL} was due to an increase in maximal conductance, with no changes in gating parameters. This also implies that I_{CaL} "window current" was unmodified by NOS1 inhibition.

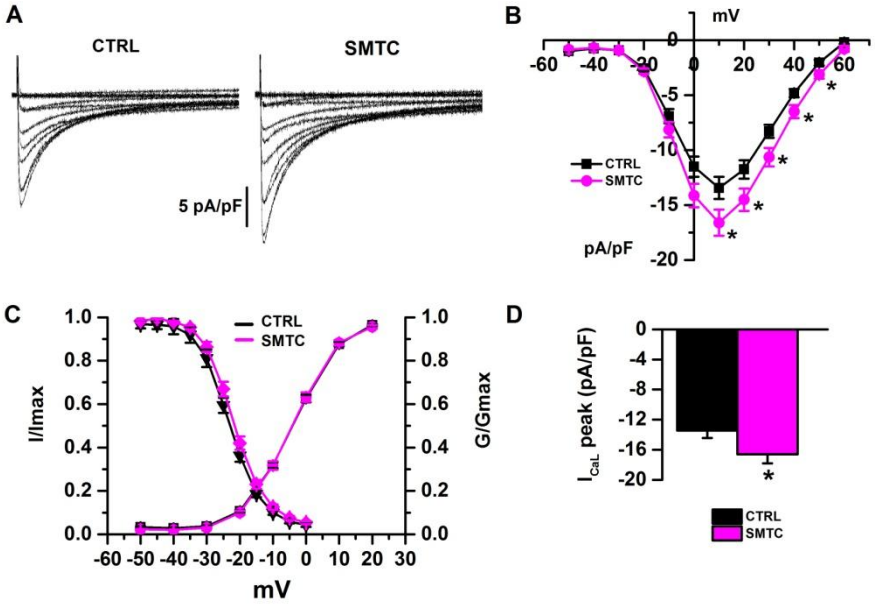

Figure 3. A) Representative traces of I_{CaL} at different voltage step from CTRL and SMTC myocytes. B) Current/voltage (I/V) relationships of I_{CaL} current density for CTRL and SMTC treated cells (CTRL n=25, SMTC n=20). C) Activation and inactivation curves of CTRL and SMTC treated cells. D) Peak density of I_{CaL}. *=P<0.05 vs CTRL.

3.3.2 *Rapidly activating delayed rectifier K^+ current (I_{Kr})*

From measurement of I_{Kr} tail amplitude, I_{max} appeared to be slightly lower in SMTC treated than in CTRL myocytes (0.89 ± 0.04 pA/pF vs 0.98 ± 0.05 pA/pF, respectively); however, the change did not achieve significance (**Figure 4.** B and C). I_{Kr} steady-state activation curve was similar between SMTC treated and CTRL myocytes (**Figure 4.** D), with no differences in the $V_{0.5}$ value (-10.9 ± 1.2 mV for SMTC vs -10.6 ± 1.3 mV for CTRL) and slope factor (5.3 ± 0.4 mV for SMTC vs 5.4 ± 0.3 mV for CTRL) between the two groups.

Taken together, these findings indicate that the effect of NOS1 inhibition on APD_{90} cannot be accounted for by I_{Kr} modulation.

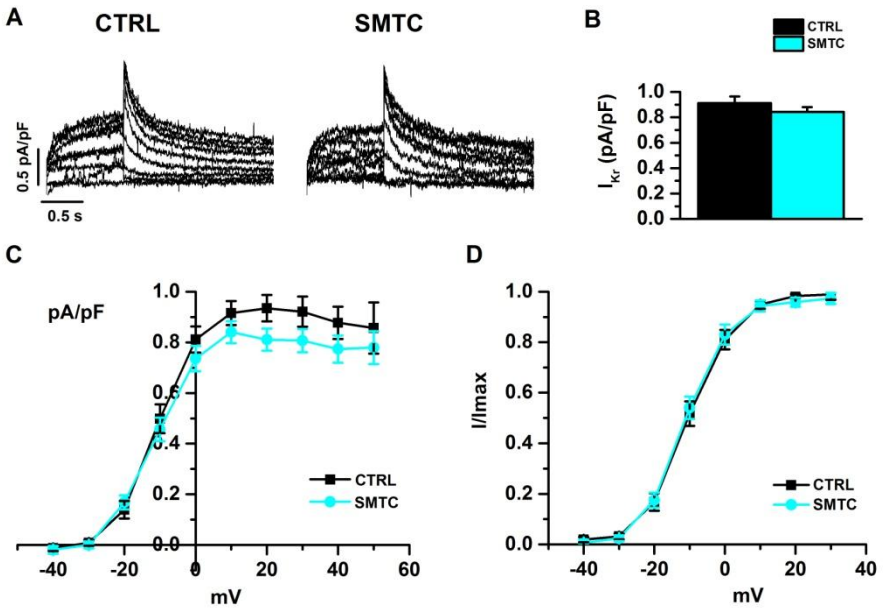

Figure 4. A) Representative traces of I_{Kr} at different voltage steps from CTRL and SMTC myocytes. B) Current density of I_{Kr} current at +10 mV from CTRL and SMTC treated cells. Current/voltage (I/V) relationships of I_{Kr} density (C) and activation curves (D) from CTRL and SMTC groups. (CTRL n=14, SMTC n=23).

3.3.3 *Slowly activating delayed rectifier K^+ current (I_{Ks})*

I_{Ks} density (measured at +40 mV in the absence of JNJ303) was comparable in SMTC and CTRL myocytes (2.5 ± 0.4 pA/pF, n=19; and 2.6 ± 0.2 pA/pF, n=16; respectively, NS. **Figure 5.** B and C). I_{Ks} mean activation curves were similar between the two groups (**Figure**

5. D). This was reflected by similarity of activation $V_{0.5}$ (16.9 ± 1.7 mV vs 14.4 ± 1.1 mV, NS) and slope factor (9.4 ± 0.6 mV vs 8.6 ± 0.5 mV, NS).

These data indicate that NOS1 inhibition did not affect I_{Ks} maximal conductance or activation and are consistent with the observation that the effect of I_{Ks} blockade (by JNJ303) was similar between SMTC treated myocytes and CTRL ones (above).

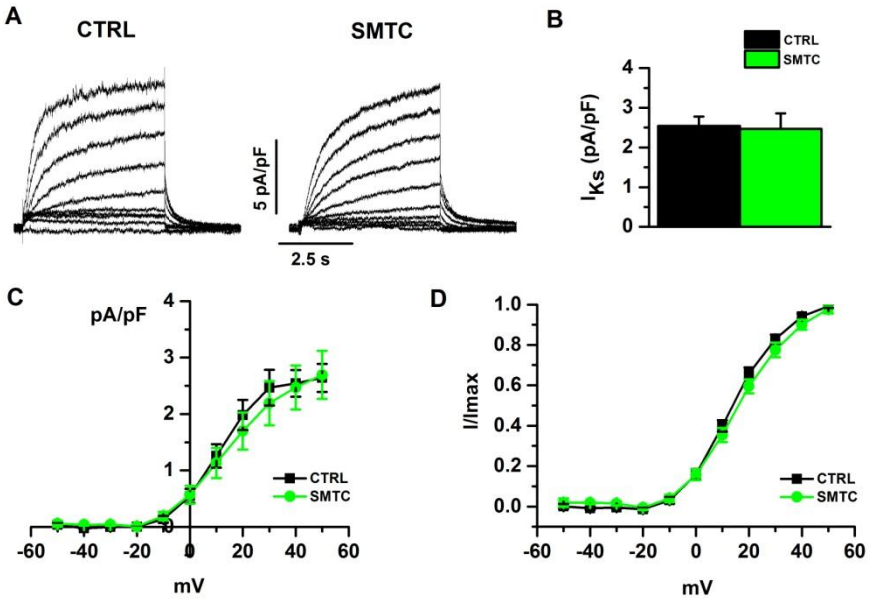

Figure 5. A) representative traces of I_{Ks} at different voltage steps from CTRL and SMTC myocytes. B) Current density at +40 mV from CTRL and SMTC treated cells. I/V relationships (C) and activation curves (D) of I_{Ks}. (CTRL n=16, SMTC n=19).

3.4 Impact of AP duration on the effects of NOS1 inhibition

According to the hypothesis formulated in the introduction, mutation-induced QT prolongation (whatever its cause) may turn SR instability (caused by NOS1 deficiency) from an asymptomatic condition into an arrhythmogenic one. The cleanest way to test this hypothesis in a general way is to evaluate the effect of different AP profiles on spontaneous Ca^{2+} release events (Ca^{2+} waves) indicative of SR instability. To this end, myocytes were V-clamped with short and long APs (AP-clamp) applied at the same cycle length (0.5 s) and I_{TI} occurrence was measured on the resulting membrane current tracings. The experiments were carried out under conditions associated with frequent DADs occurrence (SMTC + 1 nM ISO). The long AP was applied first and, when I_{TI} events were stably detected, activation was continued, within the same myocyte, with short APs. In preliminary experiments a long-long sequence of APs was applied to rule out time-dependent changes of I_{TI} occurrence.

In all myocytes showing I_{TI} occurrence during stimulation with the long AP (n=12), I_{TI} events ceased, or became markedly smaller to disappear gradually, 4-5 seconds after switching to short AP. (**Figure 6**). As a further confirmation, in a subset of cells (n=8) we applied multiple consecutive changes in APD, with a sequence of long-short-long APs. I_{TI} occurred in all myocytes stimulated with long AP (8/8 cells), ceased after switching to short AP (8/8 cells) and arose again returning to the long AP (7/8 cells).

This data confirms the hypothesis that APD prolongation, proportionally similar to that found in LQT1 patients, may act as a co-

factor in the genesis of spontaneous Ca^{2+} release events in the setting of impaired NOS1 activity.

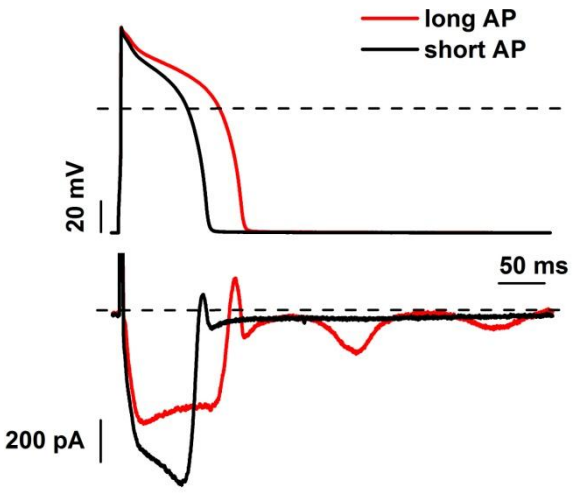

Figure 6. Long AP (APD_{90} = 140 ms, red) and short AP (APD_{90} = 100 ms, black) waveforms used as a command in AP-clamp experiments (top) and representative corresponding membrane currents induced by 1 nM ISO application in SMTC treated myocyte (bottom).

3.5 Effect of APD on Ca^{2+} load

According to the working hypothesis, in the presence of NOS1 deficiency, APD prolongation would facilitate spontaneous Ca^{2+} release events by increasing intracellular Ca^{2+} content. To test this hypothesis we measured diastolic Ca^{2+} (Ca_D) and Ca^{2+} transient amplitude (Ca_T), under AP-clamp conditions, in myocytes stimulated with long AP and then swithched to short AP. The experiments were

carried out in the presence of SMTC + ISO 1 nM, thus reproducing the conditions under which the effect of APD on I_{TI} was observed.

Ca_D and Ca_T were significantly affected by the change in APD, as these parameters were decreased after turning from long AP (Ca_D: 0.98 ± 0.02; Ca_T: 0.33 ± 0.04) to short AP (Ca_D: 0.89 ± 0.04; Ca_T: 0.27 ± 0.04; P<0.01) (**Figure 7.** B and C).

These data indicate that the prologation of APD results in increased intracellular Ca^{2+} content, and this could explain its effect of facilitating spontaneous Ca^{2+} release events reported above.

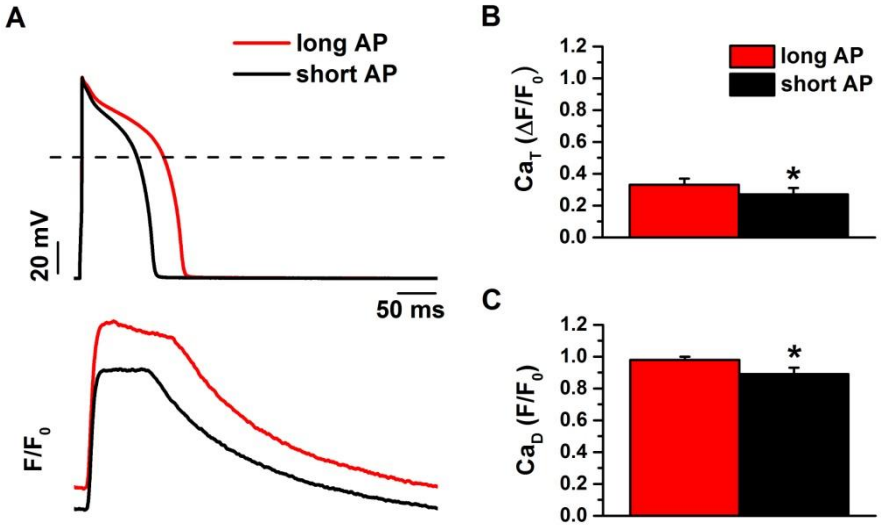

Figure 7. A) Long and short AP waveforms used as a command in AP-clamp experiments (top) and corresponding Ca^{2+} transient signals induced by 1 nM ISO application in the same SMTC treated myocyte (bottom). Analysis of diastolic Ca^{2+}, Ca_D (B), and Ca^{2+} transient amplitude, Ca_T (C) in SMTC myocytes (n=11; *=P<0.01 vs long AP).

4. Discussion

In the setting of the present study NOS1 inhibition: 1) prolonged APD_{90}; 2) increased I_{CaL}, but it affected neither I_{Kr} nor I_{Ks}; 3) increased the incidence of DADs resulting from prolonged APD and β-adrenergic stimulation. Furthermore, under NOS1 inhibition, normalization of prolonged APD prevented the occurrence of I_{TI}, the current equivalent of DADs, and this was associated to a change in diastolic Ca^{2+} and Ca^{2+} transient amplitude.

It is interesting to compare the APD prolonging effect of NOS1 blockade we observed with the APD shortening, which resulted from CAPON overexpression in the study of Chang et al. [15]. While in the present experiments, NOS1 inhibition prolonged APD by 59%, CAPON overexpression resulted in about 28% APD shortening. This difference could be explained considering that CAPON is an adaptor protein for NOS1, and acting directly on the latter may generate a greater effect than just modulating the former.

The APD prolongation induced by NOS1 inhibition could be explained as a results of the increase in I_{CaL} density. We reported an enhancement of about 24% of this current after NOS1 inhibition, result consistent with those of previous studies [8, 20], as the L-type Ca^{2+} channels are one of the major targets of NOS1, which acts as a negative feedback control system on intracellular Ca^{2+} concentration.

Moreover we also investigated the contribution to APD prolongation of other ionic currents involved in repolarization. We did not see significant alteration of the rapidly activating (I_{Kr}) and the slowly activating component (I_{Ks}) of the delayed rectifier K^+ current after

NOS1 inhibition. Therefore, our results lead us to the conclusion that the enhancement of L-type Ca^{2+} current alone seems to account for the APD prolongation observed. This is in agreement with the findings of Chang et al, who described a significant shortening of APD and a concomitant reduction in the density of I_{CaL} after CAPON overexpression, with no alteration in the delayed rectifier K^+ current, except for a slightly increase in the rapidly activating component (I_{Kr}). Taken together, the main effects of NOS1 inhibition detected in the present study are opposite to those of CAPON overexpression, thus suggesting that the function of NOS1 is closely related to CAPON activity/expression.

Here we also reported that ISO had a larger effect on APD in SMTC treated cells respecting to control ones, and this could be again explained considering that β-adrenergic stimulation *per se* increase Ca^{2+} influx through L-type Ca^{2+} channels which could be further enhanced when the modulation of these channels exerted by NOS1 activity is missing, as after SMTC treatment.

Furthermore, this condition of enhanced APD prolongation induced by β-adrenergic stimulation in SMTC myocytes was associated with increased incidence of DADs respecting to CTRL ones (93% vs 22%). DADs could be either the consequence of RyR dysfunction or induced by Ca^{2+} overload, two conditions that can lead to spontaneous Ca^{2+} release events, thus activating Ca^{2+}-sensitive membrane conductances (mainly trough NCX exchanger) and consequently inducing membrane excitation and afterdepolarizations [21]. Experimental findings showed that a more loaded SR is not the only prerequisite for the generation of aftercontractions since they can be

present or absent when the SR Ca^{2+} content is similar [22]. Thus, the loading of the SR plays a role more in determining the magnitude of Ca^{2+} release and hence the amplitude of the DAD, but the release event is initiated with a common triggering pathway that involves Ca^{2+}-induced Ca^{2+} release (CICR), as increased Ca^{2+} load of the myocytes leads to an increased Ca^{2+} level in the dyadic subspace close to RyRs which increases their open probability. [23]. Moreover, β-adrenergic stimulation itself induces rapid S-nitrosylation of proteins, notably of RyR, and this modification depends on NOS1 activity and the redox environment (ROS production). Thus, NOS1 inhibition suppresses β-adrenergic stimulated S-nitrosylation of RyR [24] and facilitates their open probability. In our experimental condition, DADs occurrence seems to be accounted by the concomitant presence of these two mechanisms. Therefore, the consequent rise in intracellular Ca^{2+} concentration, due to increase Ca^{2+} influx through I_{CaL} enhancement, may explain the increased incidence of DADs in myocytes subjected to NOS1 inhibition, particularly in a setting of RyR dysfunction, as a consequence of decrease S-nitrosylation induced by lack of NOS1 activity [11, 20]. We further observed a reduction in the time of DADs appearance after NOS1 inhibition. The more the APD was prolonged, less time it takes DADs to rise in response to β-adrenergic stimulation, possibly due to the increased intracellular Ca^{2+} concentration consequent of I_{CaL} enhancement, that could reach earlier the threshold for afterdepolarizations occurrence.

Together these findings suggest that APD prolongation and enhanced Ca^{2+} influx, facilitates spontaneous Ca^{2+} release events in a condition of SR instability, that can increase the risk for arrhythmias.

In particular, for the increased incidence of spontaneous Ca^{2+} release events, we tested the contribution of the AP duration to the effects induced by NOS1 inhibition, reporting that I_{TI} events occurring during stimulation with the long AP, ceased after switching to short AP. We concluded that this could be due to an higher Ca^{2+} load reached after stimulation with long AP compared to short AP, as diastolic Ca^{2+} and Ca^{2+} transient amplitude were both significantly affected by the change in APD. This could be explained taking in account that with the long AP, the Ca^{2+} influx is higher, thus facilitating spontaneous Ca^{2+} release events, which could be prevented, even in a setting of equal RyR dysfunction (hyponitrosylation due to SMTC treatment), after switching to the short AP, as the Ca^{2+} influx is reduced.
Therefore, our results demonstrated that in a condition in which NOS1 activity is inhibited, the duration of AP is crucial for the occurrence of Ca^{2+} release events (such as I_{TI}). This consideration, could be translated to the clinical experience, with subjects carrying the same SNP in NOS1AP gene, but with different QT interval as a discriminant: subjects with NOS1AP SNP but normal QT, that are healthy; and patients with the same variant but associated with a pathological QT prolongation, which have the LQT1 phenotype worsen.

The fact that CAPON expression is important for NOS1 activity and its correct subcellular localization is well reported in literature. Chang et al., after CAPON overexpression observed a shortening in APD and a reduction in I_{CaL} density [15], similarly to Burkard et al. which reported a reduction in I_{CaL} density after NOS1 overexpression [9]; and this is totally comparable with our opposite results presented after

NOS1 inhibition. Moreover, Treuer et al. referred a reduction in Ca^{2+} transient and S-nitrosylation after CAPON silencing [25], results similar to those presented by Gonzalez et al. for a NOS1 knockout mouse model [11]. Taken together, all these effects of CAPON modulation, mirror the results seen, in our and others work, for NOS1 direct deletion, condition characterized by defective modulation of excitation-contraction coupling (ECC) and alteration in normal Ca^{2+} handling, that facilitates Ca^{2+}-induced ventricular arrhythmias [20].
NOS1AP SNPs have been consistently associated to QTc prolongation and increased risk of cardiac events, but the functional effects of these SNPs have not been demonstrated so far. Interestingly, in a study of gene expression analysis of myocardial tissue taken from extracted pacemaker and defibrillator, Saba et al. reported that CAPON mRNA levels are decreased in patients presenting the rs10494366 and rs10918594 NOS1AP polymorphisms [26], thus suggesting that the functional effect of these variants may results in a reduction of CAPON protein expression, and further supporting our hypothesis. Therefore, taking in account our results from NOS1 inhibition and those of CAPON modulation, it's possible that the effect of NOS1AP SNPs is likely to induce a decrease in NOS1 function/localization thus compromising SR functional stability and facilitate arrhythmias in the context of prolonged repolarization (LQT1).

5. Limitations

This project is focused on the investigation of NOS1 deletion effects. Starting from the evidence of data in literature that demonstrate how CAPON modulation directly influences the activity of NOS1, here we

just infer that the effect of NOS1 inhibition we have observed, could possibly explain the functional effect of NOS1AP polymorphisms. However, we do not have the direct demonstration of this hypothesis. One possible way by which the assumption that the polymorphisms directly affect NOS1 function could be proven, is using patient's specific induced pluripotent stem cell-derived cardiomyocytes (iPSC-CMs), which have the exactly genetic background of the patients, carrying the LQT1 mutation in association with different NOS1AP SNPs.

References

1. Schwartz, P.J. and M.J. Ackerman, *The long QT syndrome: a transatlantic clinical approach to diagnosis and therapy.* Eur Heart J, 2013. **34**(40): p. 3109-16.

2. Tomas, M., et al., *Polymorphisms in the NOS1AP gene modulate QT interval duration and risk of arrhythmias in the long QT syndrome.* J Am Coll Cardiol, 2010. **55**(24): p. 2745-52.

3. Earle, N., et al., *Single nucleotide polymorphisms in arrhythmia genes modify the risk of cardiac events and sudden death in long QT syndrome.* Heart Rhythm, 2014. **11**(1): p. 76-82.

4. Wratten, N.S., et al., *Identification of a schizophrenia-associated functional noncoding variant in NOS1AP.* Am J Psychiatry, 2009. **166**(4): p. 434-41.

5. Arking, Dan E., et al. *A Common Genetic Variant in the NOS1 Regulator NOS1AP Modulates Cardiac Repolarization*. Nature Genetics, 2006. **38**(6): p. 644–51.

6. W. Post et al., *Associations between genetic variants in the NOS1AP (CAPON) gene and cardiac repolarization in the old order Amish*. Hum Hered, 2007. **64**(4): pp. 214–219.

7. Jaffrey, S.R., et al., *CAPON: a protein associated with neuronal nitric oxide synthase that regulates its interactions with PSD95.* Neuron, 1998. **20**(1): p. 115-24.

8. Sears, C.E., et al., *Cardiac neuronal nitric oxide synthase isoform regulates myocardial contraction and calcium handling.* Circ Res, 2003. **92**(5): p. e52-9.

9. Burkard, N., et al., *Conditional neuronal nitric oxide synthase overexpression impairs myocardial contractility.* Circ Res, 2007. **100**(3): p. e32-44.

10. Eu, J.P., et al., *Regulation of ryanodine receptors by reactive nitrogen species.* Biochem Pharmacol, 1999. **57**(10): p. 1079-84.

11. Gonzalez, D.R., et al., *Deficient ryanodine receptor S-nitrosylation increases sarcoplasmic reticulum calcium leak and arrhythmogenesis in cardiomyocytes.* Proc Natl Acad Sci U S A, 2007. **104**(51): p. 20612-7.

12. Wang, H., et al., *Regulation of myocyte contraction via neuronal nitric oxide synthase: role of ryanodine receptor S-nitrosylation.* J Physiol, 2010. **588**(Pt 15): p. 2905-17.

13. Zhang, Y.H., et al., *Reduced phospholamban phosphorylation is associated with impaired relaxation in left ventricular myocytes from neuronal NO synthase-deficient mice.* Circ Res, 2008. **102**(2): p. 242-9.

14. Bencsik, P., et al., *Cardiac capsaicin-sensitive sensory nerves regulate myocardial relaxation via S-nitrosylation of SERCA: role of peroxynitrite.* Br J Pharmacol, 2008. **153**(3): p. 488-96.

15. Chang, K.C., et al., *CAPON modulates cardiac repolarization via neuronal nitric oxide synthase signaling in the heart.* Proc Natl Acad Sci U S A, 2008. **105**(11): p. 4477-82.

16. A. Zaza, M. Rocchetti, A. Brioschi, A. Cantadori, and A. Ferroni, *Dynamic Ca2+-induced inward rectification of K+ current during the ventricular action potential*. Circ Res, 1998. **82**(9): p. 947–956.

17. Paavola J, Viitasalo M, Laitinen-Forsblom PJ, Pasternack M, Swan H, Tikkanen I, Toivonen L, Kontula K, Laine M., *Mutant ryanodine receptors in catecholaminergic polymorphic ventricular tachycardia generate delayed afterdepolarizations due to increased propensity to Ca2+ waves*. Eur Heart J, 2007. **28**(9): p. 1135-42.

18. M. Rocchetti et al., *Ranolazine prevents INaL enhancement and blunts myocardial remodelling in a model of pulmonary hypertension.* Cardiovasc Res, 2014. **104**(1): p. 37–48.

19. Sanguinetti, M.C., *Long QT syndrome: ionic basis and arrhythmia mechanism in long QT syndrome type 1.* J Cardiovasc Electrophysiol, 2000. **11**(6): p. 710-2.

20. Cutler, M.J., et al., *Aberrant S-nitrosylation mediates calcium-triggered ventricular arrhythmia in the intact heart.* Proc Natl Acad Sci U S A, 2012. **109**(44): p. 18186-91.

21. Noble D, Varghese A, Mod*elling of sodium-overload arrhythmias and their suppression*. Can J Cardiol. 1998. 14(**1**):97-100.

22. Tweedie, D., S.E. Harding, and K.T. MacLeod, *Sarcoplasmic reticulum Ca content, sarcolemmal Ca influx and the genesis of arrhythmias in isolated guinea-pig cardiomyocytes.* J Mol Cell Cardiol, 2000. **32**(2): p. 261-72.

23. Fink M, Noble PJ, Noble D. *Ca^{2+}-induced delayed afterdepolarizations are triggered by dyadic subspace Ca^{2+} affirming that increasing SERCA reduces aftercontractions*. American Journal of Physiology - Heart and Circulatory Physiology. 2011. 301(**3**):H921-H935.

24. A. Z. Vielma, L. León, I. C. Fernández, D. R. González, and M. P. Boric, *Nitric Oxide Synthase 1 Modulates Basal and β-Adrenergic-Stimulated Contractility by Rapid and Reversible Redox-Dependent S-Nitrosylation of the Heart*. PLoS One, 2016. **11**(8).

25. A. V. Treuer and D. R. Gonzalez, *NOS1AP modulates intracellular Ca(2+) in cardiac myocytes and is up-regulated in dystrophic cardiomyopathy*. Int J Physiol Pathophysiol Pharmacol, 2014. 6(1): p. 37–46.

26. S. Saba *et al.*, *Cardiac levels of NOS1AP RNA from right ventricular tissue recovered during lead extraction*. Heart Rhythm, 2012. **9**(3): p. 399–404.

Chapter 3

I_{Kr} impact on repolarization and its variability assessed by Dynamic Clamp.

Claudia Altomare, MS[1]; Chiara Bartolucci, PhD[2]; Luca Sala, PhD[1]; Joyce Bernardi, MS[1]; Gaspare Mostacciuolo, Mr[1]; Marcella Rocchetti, PhD[1]; Stefano Severi, PhD[2*]; Antonio Zaza, MD[1*].

[1] Department of Biotechnologies and Biosciences, University of Milano-Bicocca, Milan, Italy;

[2] Biomedical Engineering Laboratory D.E.I, University of Bologna, Cesena, Italy.

* SS and AZ equally contributed to this work.

Circ Arrhythm Electrophysiol. 2015;8(5):1265-75.

1. Abstract

Background: repolarization and its stability are exquisitely sensitive to I_{Kr} features. Information on the relative importance of specific I_{Kr} abnormalities is missing and would assist in the evaluation of arrhythmogenic risk. *Methods and Results*: in single guinea-pig myocytes, endogenous I_{Kr} was replaced by modelled I_{Kr} (mI_{Kr}) by Dynamic-Clamp (DC) at a cycle length of 1 s. mI_{Kr} parameters were systematically modified, and the resulting changes in action potential duration (APD) and its short term variability (SD1) were measured. We observed that (1) I_{Kr} blockade increased SD1 more than expected by its dependency on APD; (2) mI_{Kr} completely reversed APD and SD1 changes caused by I_{Kr} blockade; (3) repolarization was most sensitive to inactivation shifts, which affected APD and SD1 concordantly; (4) activation shifts of the same magnitude had marginal impact on APD, but only when reducing mI_{Kr}, they significantly increased SD1; (5) changes in maximal conductance resulted in a pattern similar to that of activation shifts. *Conclusions*: the largest effect on repolarization and its stability are expected from changes in I_{Kr} inactivation. APD is less sensitive to changes in other I_{Kr} gating parameters, which are better revealed by SD1 changes. SD1 may be more sensitive than APD in detecting I_{Kr}-dependent repolarization abnormalities.

2. Introduction

Abnormalities of the rapid component of the delayed rectifier K^+ current ($I_{Kr,}$ HERG channel) are associated with remarkable prolongation and instability of repolarization. Both these conditions entail arrhythmic risk [1], as epitomized by the phenotype of HERG loss-of-function mutations (type 2 Long-QT syndrome; LQT2).

One of the major challenges of translational electrophysiology remains prediction of the functional phenotype associated with a given channel abnormality. Even once specific functional defects have been identified in heterologously expressed channels, their impact on cell electrical activity remains difficult to predict. This is because the action potential (AP) is determined by feedback interplay between membrane potential, many current components, intracellular Ca^{2+} and, likely, further unknown factors. Dynamic clamp (DC) is a promising approach to this problem because it allows to test how the properties of a numerically modelled current affect the AP generated by a real myocyte [2, 3]. An individual ionic current is orders of magnitude simpler to model that the whole AP; thus, DC is expectedly more reliable than whole AP modeling in predicting the outcome of a current abnormality.

This work exploits DC to systematically analyze the effect of changes in I_{Kr} conductance and gating properties on guinea-pig AP duration (APD) and its time-variability, an index of electrical instability [1, 4-5]. The results provide information, potentially of general value, on the weight of individual I_{Kr} gating features in determining

repolarization course and stability. Once clinically validated, such information might be instrumental to risk assessment and clinical management of I_{Kr} mutations; indeed, although reduced channel expression is the commonest mutation-induced derangement, gating abnormalities are also represented (examples given in Table I in the Data Supplement), and their consequences are more difficult to predict.

3. Methods

3.1 Cell isolation

Dunkin-Hartley Guinea pigs were euthanized by cervical dislocation under 800 mg/Kg chloral hydrate intraperitoneal anesthesia. Ventricular myocytes were isolated by using a retrograde coronary perfusion method previously published [6], with minor modifications. Rod-shaped, Ca^{2+}-tolerant myocytes were used within 12 h from dissociation. This investigation conforms to the Guide to the Care and Use of Laboratory Animals published by the US National Institutes of Health (NIH publication no. 85-23, revised 1996) and to the guidelines for Animal Care endorsed by the University of Milano-Bicocca.

3.2 I_{Kr} numerical model

A deterministic, Hodgkin-Huxley-type (HH), model of I_{Kr} was developed by optimizing the Luo-Rudy model [7, 8] against I_{Kr}

profile recorded under AP-clamp conditions. To this end, we developed a parameter optimization routine based on the least square difference between experimental and simulated I_{Kr} time courses during AP-clamp. Inactivation and its recovery were considered instantaneous and activation/deactivation monoexponential as in the Luo-Rudy model. Preliminary simulations (Figure I and II in the Data Supplement) indicated that this simplification slightly changed peak I_{Kr} amplitude, but failed to impact on APD. Model code was implemented by using the Real-Time eXperiment Interface (RTXI; www.rtxi.org). Baseline model parameter values are listed in Table II in the Data Supplement, and their modifications are described in the relevant sections of Results.

3.3 Electrophysiology

Recordings were performed on single myocytes superfused with standard Tyrode's solution (Table III in the Data Supplement) by patch clamp in the whole-cell configuration at 36.5 °C. Ca^{2+} and EGTA concentrations were calculated to achieve free pipette Ca^{2+} = 10^{-7} mol/L with minimal buffering of systolic transients, as indicated by persistence of sharp myocyte contractions. I_{Kr} was completely and selectively blocked by 5 μmol/L E4031 [9] added to Tyrode solution.

APs were recorded (I-clamp mode) at pacing cycle length (CL) of 1s and subsequently applied at the same CL as command potential in V-clamp mode (AP-clamp), as previously described [10]. I_{Kr} was identified as E4031-sensitive current (I_{E4031}) after achievement of steady-state block. I_{E4031} profile was then used as a template for

optimization of I_{Kr} model parameters [11]. Adequacy of pipette seal was verified at the beginning of each experiment. Myocytes in which diastolic potential changed by > 2 mV during experimental protocol were discarded.

3.4 Dynamic clamp

In DC, APs, recorded from the myocytes, were acquired at a sampling rate of 5 KHz into the computer to drive the numerical I_{Kr} model. Modeled I_{Kr} (mI_{Kr}) was calculated in real-time (within one sampling interval) and injected into the myocyte during continued AP recording. Endogenous I_{Kr}, blocked by E4031, was thus replaced by mI_{Kr}, while leaving in place all the other determinants of myocyte electric activity. APs were recorded at a CL = 1 s for at least 3 minutes after achieving a steady AP profile. 5 µmol/L E4031 was then applied to block endogenous I_{Kr}. mI_{Kr} injection was then activated (under continuous E4031 superfusion) and the resulting AP changes recorded.

After verifying that mI_{Kr} injection restored the AP to control profile, the relevant model parameters were changed and the ensuing AP changes recorded within the same myocyte. APD variability measurements (SD1 and SD2, see subsequent subsection) were performed over at least 40 beats after AP profile had fully adapted under each condition.

3.5 Data analysis and statistics

APD was measured at the 90% repolarization level; beat-to-beat measurements were automatically performed by a custom software routine.

SD1 (ms, also referred to as STV) [12], graphically defined in APD_n versus APD_{n+1} (Poincaré) plots as the mean of orthogonal deviations from the identity line, was calculated as [12]:

$$SD1 = \Sigma(|APD_{n+1} - APD_n|)/[n_{beats} \times \sqrt{2}] \quad \textbf{(1)}$$

where APD_n and APD_{n+1} indicate APD of the n^{th} and $n+1^{th}$ APs respectively, and n_{beats} denotes the total number of consecutive beats analyzed.

SD2 (ms, also referred to as LTV) [12], graphically defined in Poincaré plots as the mean of deviations along the identity line, was calculated as [12, 13]:

$$\Sigma(|APD_{n+1} + APD_n - 2APD_{mean}|)/[n_{beats} \times \sqrt{2}] \quad \textbf{(2)}$$

According to a numerical analysis presented in Figure III in the Data Supplement, although both SD1 and SD2 are measures of variability, their ratio (SD1/SD2) is independent from variability magnitude, but proportional to its frequency content. Put in simple terms, whereas a high SD1/SD2 ratio indicates prevalence of beat-to-beat APD

variability (SD1/SD2= ∞ in 1:1 alternans), a low one implies that a larger number of cycles is required for the same APD change (see Figure III in the Data Supplement for more detail). Whereas SD1 and SD2 are correlated in most circumstances, SD1/SD2 carries independent information; therefore, variability will be expressed in terms of SD1 and SD1/SD2 ratio.

To analyze I_{Kr} distribution during the AP, repolarization was divided in 3 phases: Phase 1: the quasi-linear plateau phase, Phase 3: the quasi-linear terminal fast repolarization; and Phase 2: the transition between these two phases. Proximal and distal boundaries of each quasi-linear phase were determined with a custom-made recursive routine (i.e. in an operator-independent manner) detecting divergence from linearity [11].

Boundaries of the interposed phase 2 were set accordingly. Mean current (I_{mean}) within each phase was calculated as

$$I_{mean} = \frac{\int_{t1}^{t2} I*dt}{(t_2 - t_1)} \quad \textbf{(3)}$$

where t_1 and t_2 are phase boundaries.

Means were compared by paired *t* test or ANOVA, as appropriate; Bonferroni's test was used for adjusting significance cut-off in multiple post-hoc comparisons. Correlation and regression coefficients were estimated by linear models (GraphPad Prism 5).

P<0.05 was used to define significance. Data are presented as mean±SEM.

4. Results

4.1 I_{E4031} replacement by mI_{Kr}

APs were recorded at a CL of 1 s (Figure 1) in control conditions (ctr). E4031 superfusion prolonged APD (+ 10.4 ± 2.1 %; *P*<0.05). As can be visually appreciated from Poincaré plots, E4031 significantly increased SD1 only (+ 38.6 ± 5.6 %; *P*<0.05) and SD1/SD2 became accordingly larger (+ 33.1 ± 10.4 %; *P*<0.05). This indicates that I_{Kr} blockade preferentially augmented the faster (beat-to-beat) component of APD variability. DC was then activated in the continuing presence of E4031 and mI_{Kr} was injected. This shortened APD by 13.1 ± 1.5% and fully restored AP profile to make it precisely overlap control one (inset Figure 1A). mI_{Kr} injection reduced SD1 (-31.1 ± 3.2 %; *P*<0.05 versus E4031) back to control (NS versus control) and SD2 below control (-10.6 ± 6.2 %; *P*<0.05 versus control). Thus, mI_{Kr} failure to restore SD1/SD2 was only apparent, reflecting further elimination of a slower component of variability, rather than the persistence of the faster component. Only for this subtle aspect mI_{Kr} diverged from native I_{Kr}. Results in all aspects similar to those obtained at CL of 1000 ms were also obtained at CLs of 250 ms and 3000 ms, as reported in Figure IV in the Data Supplement.

Figure 1

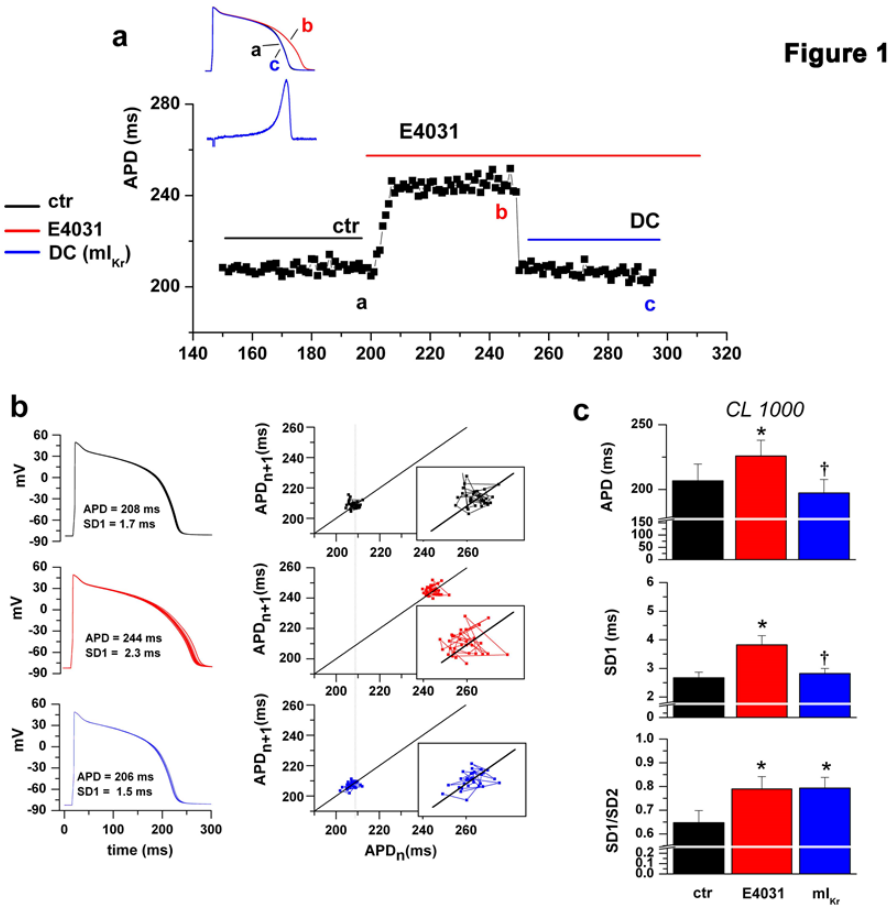

Figure 1. mI_{Kr} injection reverses E4031 effects. A, Representative time series of APD in control (a, black), during superfusion of E4031 (b, red) and during injection of mI_{Kr} (c, blue). In the inset, example of red and blue traces showing the injection of $mI_{Kr,}$ which reverses APD prolongation in the presence of E4031; **B,** Ten AP-aligned waveforms, recorded in the 3 conditions, are shown with APD and SD1 average values; Poincaré plots, in parallel, evidence the dispersion of all APD values respect to the identity line (insets) and the mean APD referred to the control condition (dot line). C, statistics of APD, SD1 and SD1/SD2in all experimental conditions (P<0.05; *vs* ctr, †*vs* E4031; n= 23). AP indicates action potential; APD, action potential duration; DC, dynamic clamp; SD1, orthogonal APD variability; and SD2, longitudinal APD variability.

4.2 Correlation between APD and its variability

Proportionality between SD1 and mean APD is an intrinsic system property (see introduction) and can thus be expected. To investigate whether such proportionality was perturbed by I_{Kr} blockade and restored to control by mI_{Kr} injection, single SD1 values recorded under the 3 conditions (control, E4031, mI_{Kr}) were pooled and plotted against the corresponding mean APD values (Figure 2A). Pooled data were then fitted by a linear function and raw residuals (i.e. with their sign; rR) were summed separately for each condition. Bar graphs (Figure 2B) show that the sum of raw residuals (ΣrR) was negative for control and mI_{Kr} to become large and positive for E4031. This implies that, under I_{Kr} blockade, SD1 dependency on mean APD deviated from the general pattern. SD1 versus APD relationships were then fitted separately for each condition. The regression intercept was similar between control and mI_{Kr}, but larger for E4031 ($P<0.05$ versus control, linear regression GraphPad Prism 5); although the regression slope tended to be larger for E4031, the difference did not achieve significance (Figure 2C). This indicates that, under I_{Kr} blockade, SD1 was larger than expected from its intrinsic dependency on mean APD. Nevertheless, mI_{Kr} injection restored the control pattern; thus, the stabilizing effect of I_{Kr}, unveiled by this analysis, was necessarily based on I_{Kr} properties represented in the numerical model.

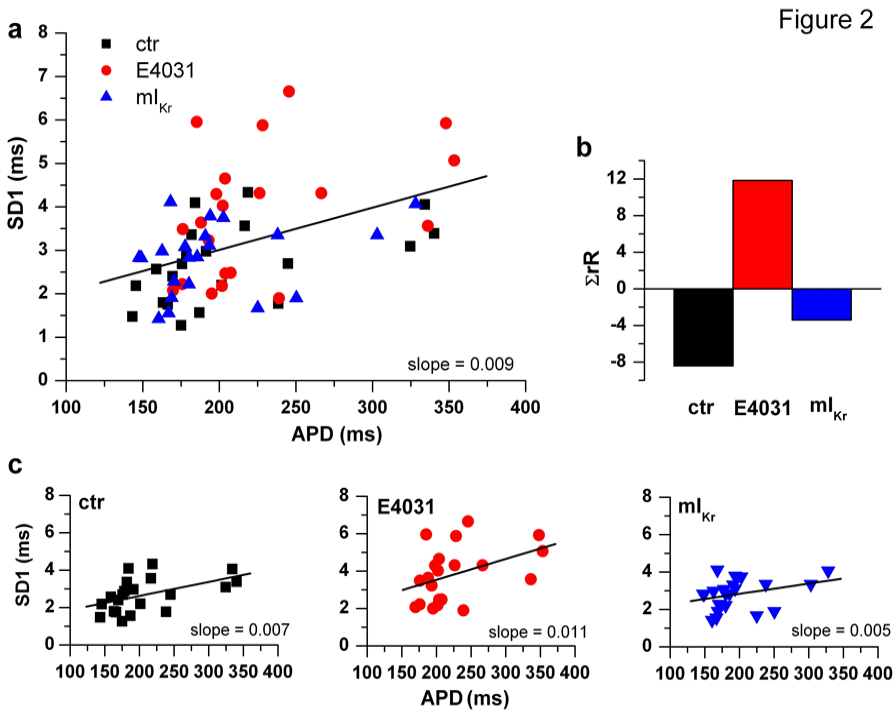

Figure 2. APD vs SD1 correlation. **A,** Plot of data pooled from all experimental conditions with the overall regression line. **B,** Sum of raw residuals (ΣrR) from the plot in **A**. **C**, Plots of data for each condition with the respective regression lines. APD indicates action potential duration; and SD1, orthogonal APD variability.

4.3 Impact of mI_{Kr} features on APD and its variability

In this section, different mI_{Kr} versions were prepared by changing gating parameters symmetrically around their value obtained from model optimization (control). The different models were applied under DC in the presence of E4031; APD and SD1 were measured from 40 APs in each condition; in all figures, control is represented in black, the negative parameter change in red and the positive change in blue. Maximal conductance (g_{max}), mid-potentials for steady-state

activation ($V_{0.5}A$) and inactivation ($V_{0.5}I$) and activation/deactivation time-constant (τ) were considered.

4.3.1 Changes in maximal conductance (g_{max})

To evaluate the impact of I_{Kr} conductance, g_{max} was changed by ± 30 % (± Δ) from its control value (0.032 mS/µF).

A representative example of the effect of g_{max} changes in a single myocyte is shown in Figure 3A-3C. Figure 3A shows time series of APD values under control (0.032 mS/µF), -Δ and +Δ. In this myocyte, -Δ did not change APD appreciably, but increased its variability; +Δ slightly reduced APD, but not its variability (average APD and SD1 values for this myocyte are shown under the traces in Figure 3B). Figure 3C illustrates average mI_{Kr} profile of the myocyte under the 3 conditions; mI_{Kr} is plotted as function of time (I/t plot aligned with the corresponding average AP waveform) and as a function of V_m (I/V plot). The increase in mI_{Kr} amplitude can be appreciated from both plots. The I/V plot shows that g_{max} changes simply scaled current amplitude (I_{peak}), without affecting current profile; indeed, the voltage at which mI_{Kr} was maximal was unchanged (V_{peak}; Table). Therefore, the apparent shift of mI_{Kr} observed in the I/t plot was secondary to the slight AP shortening/prolongation occurring in this myocyte.

Statistics from 15 cells (Figure 3D) indicate that a 30% decrease of g_{max} did not affect APD significantly, but caused an appreciable increase of both SD1 (red versus black) and SD2, SD1/SD2 remaining

unchanged (Table). Neither APD nor its variability was significantly changed by a g_{max} increment of the same magnitude (+Δ).

Figure 3

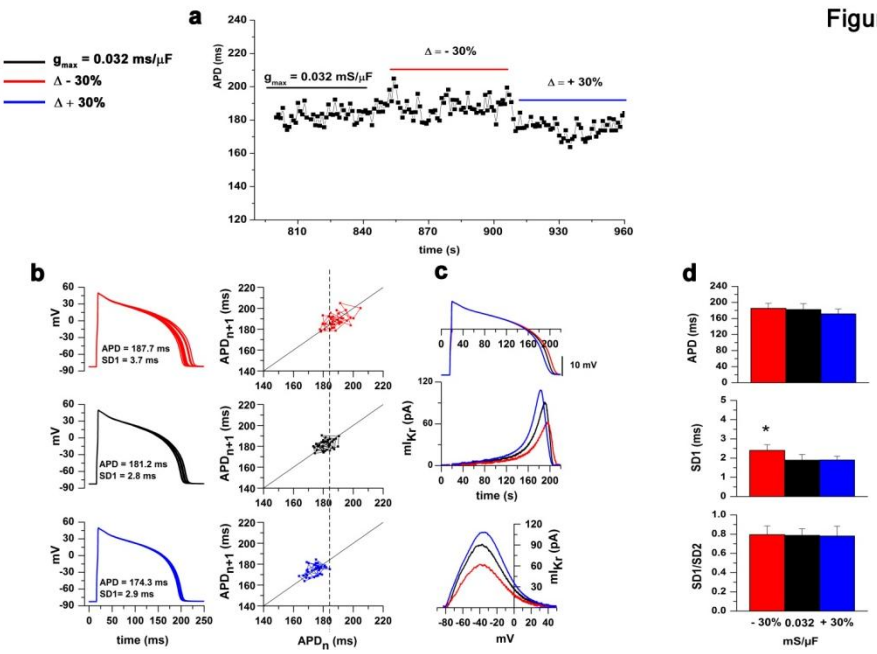

Figure 3. Changes in maximal conductance. Recordings performed at 3 values of g_{max} (0.032 mS/µF and Δ ± 30% in color) are shown. **A,** example of 40 APD over time. **B**, 10 AP aligned waveforms are shown with APD and SD1 average values. Poincaré plots, in parallel, evidenced the dispersion of all APD values respect to the identity line and the mean APD referred to the control condition (dot line). **C**, mI_{Kr} profile aligned with the corresponding average AP waveform represented as I/t and I/V_m plots. **D**, statistics of APD, SD1, and SD1/SD2 in all experimental conditions (**P*<0.05 *vs* ctr, n = 11). AP indicates action potential; APD, action potential duration; SD1, orthogonal APD variability; and SD2, longitudinal APD variability.

Table 1: effect of changes in model parameters (g_{max}, $V_{0.5}A$, τA, $V_{0.5}I$) on mI_{Kr} features, APD and its variability.

Model parameters	-Δ	DC	+Δ	# cells
g_{max} (mS/µF)	**-30%**	**0.032**	**+30%**	
V_{peak} (mV)	-40.8 ± 0.47	-41.7 ± 0.24	-41.8 ± 0.21	
I_{peak} (pA/pF)	0.69 ± 0.04*	0.91 ± 0.04	1.24 ± 0.03 *	≥ 8
TTP (ms)	196.3 ± 12	196.5 ±11.9	180.4 ± 11.4*	
$V_{0.5}A$	**-15 mV**	**-20.6**	**+15 mV**	
V_{peak} (mV)	-41.8 ± 1.4	-41.6 ± 0.3	-33.5 ± 0.26*	
I_{peak} (pA/pF)	0.97 ± 0.01*	0.93 ± 0.01	0.76 ± 0.01*	= 8
TTP (ms)	182.2 ± 13	175.9 ±11.3	177.5 ± 13.7	
$V_{0.5}I$	**-15 mV**	**-30.7**	**+15 mV**	
V_{peak} (mV)	-49.7 ± 0.38*	-41.5 ± 0.24	-31.3 ± 0.17*	
I_{peak} (pA/pF)	0.66 ± 0.004*	0.97 ±0.007	1.33 ± 0.003*	≥ 7
TTP (ms)	184.3 ± 10.1	172.6 ±11.5	133.9 ± 7.04*	
τA	**100 ms**	**270**	**400 ms**	
V_{peak} (mV)	-39.6 ± 0.5*	-42 ± 0.1	-42.6 ± 0.1	
I_{peak} (pA/pF)	0.88 ± 0.01*	0.96 ± 0.01	0.98 ± 0.01	≥ 5
TTP (ms)	163.5 ± 12	164.6 ±10.9	166 ± 12.9	

APD indicates action potential duration at 90% repolarization; DC, dynamic clamp; SD1, orthogonal APD variability; SD2, longitudinal APD variability (see methods); TTP, time to I_{peak}; and V_{peak}, V at peak mI_{Kr} (I_{peak}). *P<0.05 vs DC.

4.3.2 Changes in mid-activation voltage ($V_{0.5}A$)

To evaluate the impact of changes in the V-dependency of steady-state activation, the midpoint of the mI_{Kr} activation curve ($V_{0.5}A$) was shifted by ± 15 mV (± Δ) from its control value (-20.6 mV). According to simple reaction kinetics, shifts in the distribution of states at equilibrium may be associated to similar shifts in the velocity of transitions between states. Therefore, the curves defining V-dependency of activation time constants (τ) were concomitantly shifted by ±15 mV (Figure 4A). The less likely alternative condition, in which shifts in steady-state activation occur without concomitant changes in V-dependency of τ, was tested in a separate series of experiments reported in Figure V in the Data Supplement.

An example of the effect of changes in $V_{0.5}A$ is shown in Figure 4B-4D. Figure 4B shows time series of APD values under control (-20.6 mV), -Δ and +Δ. In this myocyte, +Δ slightly prolonged APD and measurably increased its variability; -Δ failed to affect APD and its variability appreciably. Figure 4D illustrates the average mI_{Kr} profile of the myocyte under the 3 conditions. The I/V plot shows that mI_{Kr} profile was markedly changed by +Δ and, to a lesser extent, by -Δ. Indeed, +Δ, decreased peak mI_{Kr} and shifted V_{peak} to less negative potentials (P<0.05); -Δ only slightly increased mI_{Kr} availability at potentials corresponding to repolarization phase 3 (I_{peak} and V_{peak} in Table). Because of the small changes in APD, mI_{Kr} traces almost overlap in the I/t plot, where only a change in peak current amplitude can be appreciated for +Δ.

Statistics from 8 cells (Figure 4E) indicated that a -15 mV shift in $V_{0.5}A$ (accompanied by shifts in τ curves) failed to affect APD, SD1 and SD1/SD2significantly. A positive shift in $V_{0.5}A$ also failed to affect APD, but increased SD1; SD1/SD2 also showed a trend to increase, very close to statistical significance.

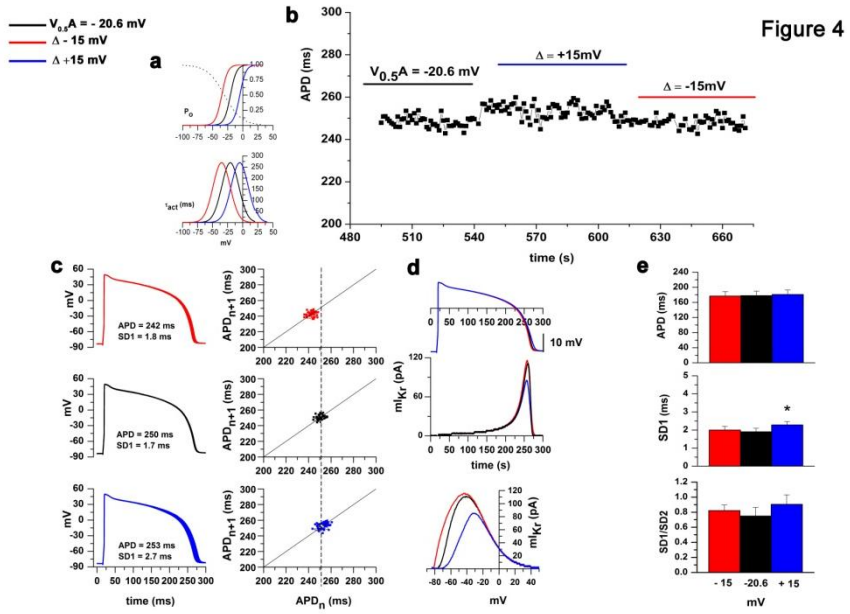

Figure 4. Changes in steady-state activation. Recordings performed at $V_{0.5}A$ = -20.6 mV and with Δ ± 15 mV are shown. **A**, Steady-state activation (*P*o) and $\tau_{act/deact}$ V-dependency curves computed by the model in 3 conditions (color); inactivation curves are superimposed as dot line. **B**, Representative time course of APD recorded at 3 values of $V_{0.5}A$. **C**, Example of 10 APs for each conditions with relative APD and SD1 values and Poincaré plot at the right of panel; ctr APD is evidenced as dot line. **D**, mI_{Kr} profile aligned with the corresponding average AP waveform represented as I/t and I/V_m plots. **E**, Statistics of APD, SD1, and SD1/SD2in all experimental conditions (**vs* control value; *P*<0.05, n = 8). AP indicates action potential; APD, action potential duration; SD1, orthogonal APD variability; and SD2, longitudinal APD variability.

4.3.3 Changes in mid-inactivation voltage ($V_{0.5}I$)

To evaluate the impact of changes in the V-dependency of steady-state inactivation, the midpoint of the mI_{Kr} inactivation curve ($V_{0.5}I$) was shifted by ± 15 mV (± Δ) from its control value (-30.7 mV, Figure 5A, black line). Because mI_{Kr} inactivation was instantaneous, no kinetic considerations apply to this section.

An example of the effect of changes in $V_{0.5}I$ is shown in Figure 5B-5D. Figure 5B shows time series of APD values under control (-30.7 mV), -Δ and +Δ. -Δ strongly prolonged APD and its variability; +Δ produced quantitatively similar changes but of opposite direction, that is, it shortened APD and decreased its variability. Figure 5D illustrates average mI_{Kr} profile under the 3 conditions; mI_{Kr} is plotted as function of time and as a function of V_m (I/V plot). The I/V plot shows that, at variance with activation (above), positive and negative shifts of inactivation changed mI_{Kr} profile almost symmetrically. According to statistics from 10 myocytes, +Δ increased peak mI_{Kr} (P<0.05) and shifted V_{peak} by +10.2 mV (P<0.05); -Δ decreased peak mI_{Kr} (P<0.05) and shifted V_{peak} by – 8.2 mV (P<0.05), that is, to a value corresponding to the steeper portion of phase 3 repolarization (I_{peak} and V_{peak} in Table). As shown in Figure 5E, this resulted in significant concordant changes in both APD and SD1 (when APD prolonged SD1 increased and viceversa). SD1/SD2was unchanged in the case of -Δ, and showed only a trend to decrease for +Δ.

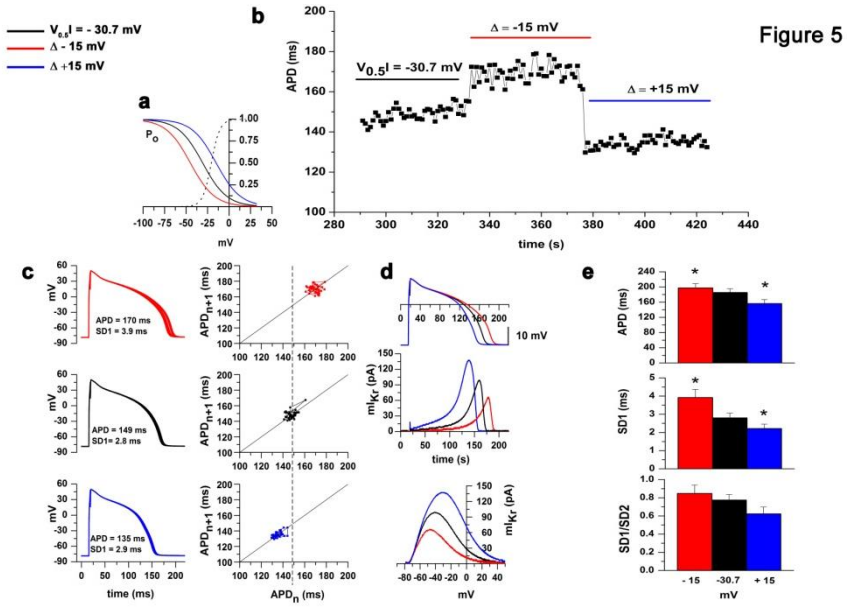

Figure 5. Changes in steady-state inactivation. Recordings performed at $V_{0.5}A$ = -30.7 mV and with Δ ± 15 mV are shown. **A**, Steady-state inactivation (*Po*) V-dependency curves computed by the model in 3 conditions (color); activation curve are superimposed as dot line. **B**, Representative time course of APD recorded at 3 values of $V_{0.5}I$. **C**, Example of 10 APs for each conditions with relative APD and SD1 values and Poincaré plot at the right of panel; ctr APD is evidenced as dot line. **D**, mI_{Kr} profile aligned with the corresponding average AP waveform represented as I/t and I/V_m plots. **E**, Statistics of APD, SD1 SD1/SD2 in all experimental conditions (**vs* control value; *P*<0.05, n=12). AP indicates action potential; APD, action potential duration; SD1, orthogonal APD variability; and SD2, longitudinal APD variability.

4.3.4 Changes in activation/deactivation time constant (τ)

To evaluate the impact of I_{Kr} activation/deactivation kinetics, the time constant (τ) was scaled at all potentials to 400 ms (+Δ) or 100 ms (-Δ) from its control value (270 ms, Figure 6, black line). All the

parameters analyzed in the previous sections were not affected by the changes in τ, except for the voltage at which peak mI_{Kr} was achieved (V_{peak}), which was shifted from -42 ± 0.1 to -39.6 ± 0.5 mV by -Δ (n=5 P<0.05) and was unaffected by +Δ.

Statistics from 10 cells (Figure 6E) indicated that these rather wide τ changes did not measurably affect APD, SD1 or SD1/SD2.

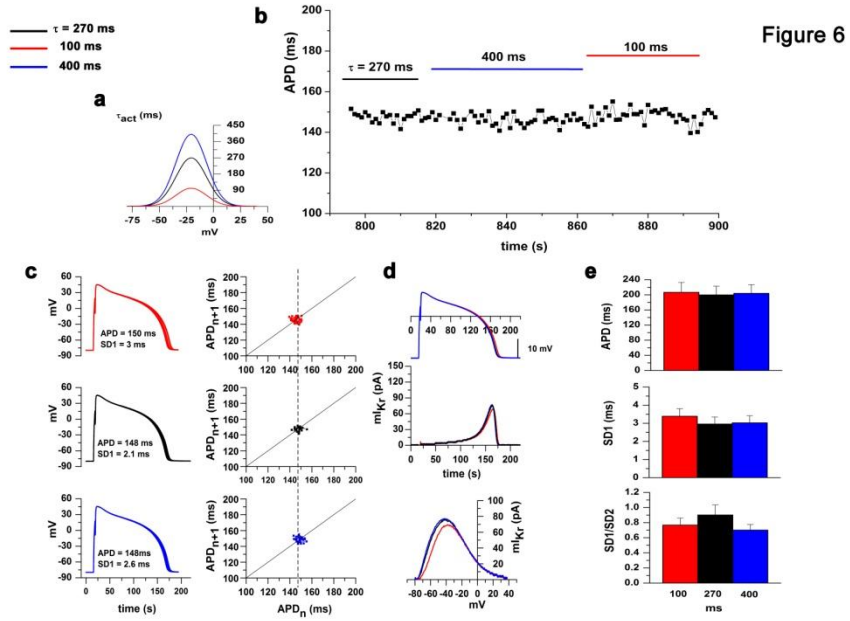

Figure 6. Changes in activation/deactivation kinetics. Recordings performed at τ = 270, 100 and 400 ms are shown. **A**,$\tau_{act/deact}$ V-dependency curves computed by the model (color). **B**, Representative time course of APD recorded at 3 values of τ. **C**, Example of 10 APs for each conditions with relative APD and SD1 values and Poincaré plot at the right of panel; ctr APD is evidenced as dot line. **D**, mI_{Kr} profile aligned with the corresponding average AP waveform represented as I/t and I/V_m plots. **E**, Statistics of APD, SD1 and SD1/SD2 in all experimental conditions (*vs control value; P<0.05, n=8). AP indicates action potential; APD, action potential duration; SD1, orthogonal APD variability; and SD2, longitudinal APD variability.

4.3.5 Changes in mI_{Kr} distribution during repolarization

Repolarization course was divided in 3 phases, as described in Methods and shown at the top of Figure 7. mI_{Kr} present within each phase was quantified as mean current (I_{mean}) in a representative subset of myocytes (n=5). Figure 7A reports the changes of I_{mean} produced within each phase (1, 2 or 3) by changes in mI_{Kr} parameters; the corresponding changes in overall I_{mean} ($I_{mean\ tot}$) are shown in the insets of each panel. Under baseline conditions (black), I_{mean} increased from phase 1 to 3. Modulation of g_{max} (left; -Δ red, +Δ blue) similarly affected I_{mean} throughout the 3 phases; the effect was asymmetrical, that is, larger for g_{max} reduction. Modulation of $V_{0.5}A$ (center), almost exclusively concerned I_{mean} during Phase 3, with larger effect resulting from the positive shift (blue). Modulation of $V_{0.5}I$ affected to some extent I_{mean} during all phases but, unlike g_{max}, sharply prevailed during Phase 1; negative (red) and positive (blue) $V_{0.5}I$ shifts exerted roughly symmetrical effects.

Comparison of Figure 7A with Figure 7B illustrates how the above I_{mean} distribution patterns impact on APD and SD1 modulation (shown in Figures 3-6), represented for this purpose as % change from baseline values. For all parameters, the extent of APD changes correlated with changes in I_{mean} during Phase 2. On the other hand, the extent of SD1 changes correlated with changes in I_{mean} during Phase 3. The format used in Figure 7B also highlights that, whereas significant changes in APD were achieved only by modulating $V_{0.5}I$, SD1 was affected by modulation of all parameters. Furthermore, the effects of

symmetrical changes in g_{max} or $V_{0.5}A$ produced strongly asymmetrical effects on SD1.

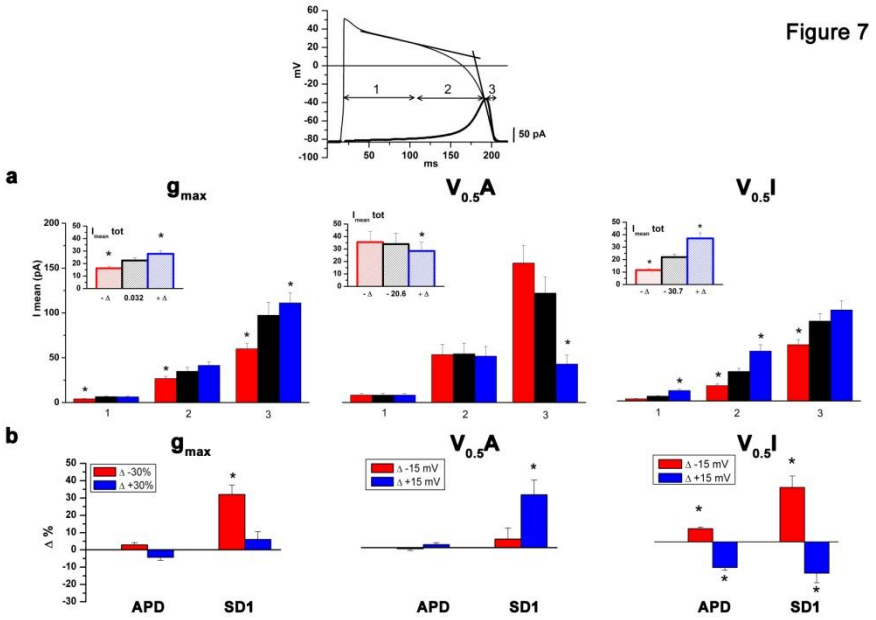

Figure 7. Relationship between mI_{Kr} distribution and repolarization changes**.** Quantification of mI_{Kr} (I_{mean}) during 3 AP phases (1, 2 or 3 as shown at the top). **A**, effect of changes (Δ) in mI_{Kr} parameters (g_{max}, $V_{0.5}A$, $V_{0.5}I$) on I_{mean} within each AP phase (black, baseline; red, – Δ and blue, + Δ); changes in overall I_{mean} ($I_{mean\ tot}$) are shown in the inset of each panel (n=5). **B**, Response of APD and SD1 (as Δ% vs control) to changes in mI_{Kr} parameters (as above). **P*<0.05 vs baseline. AP indicates action potential; APD, action potential duration; SD1, orthogonal APD variability; and SD2, longitudinal APD variability.

5. Discussion

The main findings of this study include the following: (1) injection of modeled I_{Kr} (mI_{Kr}) fully reversed the increments in APD and its variability induced by I_{Kr} blockade; (2) repolarization was most sensitive to inactivation shifts, which concordantly affected APD and its variability; (3) similar changes in activation gating had marginal impact on APD but, when leading to mI_{Kr} decrement, significantly increased APD variability; (4) a similar pattern was observed for changes in maximal conductance; and (5) even if SD1 showed a clear-cut dependency on APD, I_{Kr} blockade increased SD1 more than expected by APD prolongation alone (Figure 2); moreover, some among I_{Kr} perturbations changed SD1 without affecting APD significantly.

A question addressed by the present study is whether some yet unidentified properties of HERG channels may account for the major impact of I_{Kr} modulation on APD and its stability. Adequacy of mI_{Kr} injection in reversing the effects of endogenous I_{Kr} blockade suggests that I_{Kr} properties incorporated in the model are sufficient to account for I_{Kr} functional contribution, except for what concerns the frequency content of APD variability (mI_{Kr} failed to restore SD1/SD2, Figure 1C). The present results also show that rather substantial changes in I_{Kr} V-dependency, for example, those caused by activation shifts (Figure 4), may have a negligible impact on APD. Therefore, mean APD is a rather lax reporter of I_{Kr} abnormalities, APD variability being remarkably more sensitive. Notably, a fully deterministic I_{Kr} model, such as mI_{Kr}, also reversed the effects of endogenous I_{Kr}

blockade on APD variability. This might suggest that the latter may not arise primarily from intrinsic (stochastic) I_{Kr} variance; however, specifically designed experiments may be required to define this aspect.

As previously reported [13], I_{Kr} blockade increased APD variability, mainly its beat-to-beat component (increased SD1/SD2). mI_{Kr} restored SD1 but not the SD1/SD2 ratio; this was because mI_{Kr} returned SD1 to control values, but further reduced SD2 ($P<0.05$, not shown). This observation may suggest failure of mI_{Kr} to reproduce sensitivity of native I_{Kr} to yet unidentified factors exerting their effect over multiple cycles (e.g. changes in the intracellular milieau) and thus contributing mostly to SD2.

SD1 has been identified as a powerful predictor of Torsade de Pointes [13], leading to the suggestion that beat-to-beat APD variability may favor arrhythmogenesis. However, because of their strong correlation (see Figure III in the Data Supplement), SD1 and SD2 can hardly discriminate between beat-to-beat and slower forms of APD variability. Indeed, their ability to identify torsadogenic conditions is reported to be at least grossly similar by other studies [12, 13]. The numerical simulation reported in Figure III indicate that the SD1/SD2 ratio may provide a better chance to identify changes in beat-to-beat variability selectively; however, its prognostic value remains to be assessed.

The strong and concordant sensitivity of APD and its variability to inactivation shifts points to rectification as the I_{Kr} gating property which, if altered, is most likely to result in overt repolarization

abnormality in guinea-pig myocytes. Notably, APD shortening by positive inactivation shift was larger than APD prolongation resulting from the symmetrical negative shift (Figure 5B and 5E); this is consistent with incomplete rectification being the only mechanism thus far identified for Short-QT syndromes linked to HERG mutations [14]. SD1 changes were more conspicuous for the negative inactivation shift instead (Figure 5B and 5E), thus reinforcing the view that effects on APD and on its variability are not necessarily concordant. Negative inactivation shifts are a common feature of the subset of type 2 Long-QT syndrome mutants in which loss of function is caused primarily by gating abnormalities, that is, those in which channel density is preserved [15].

When including shifts in τ V-dependency, activation shifts had a clearly discernible effect on mI_{Kr} I/V plots, but a surprisingly small one on APD (Figure 4E). Nevertheless, the positive shift, which resulted in a clear-cut reduction in peak mI_{Kr}, significantly increased SD1. Notably, when the V-dependency of τ remained unchanged, the effects of activation shifts on SD1 disappeared, thus suggesting the importance of parallel changes in steady-state and dynamical behavior. Overall, changes in activation/deactivation gating affected I_{Kr} during Phase 3 only (Figure 7A); indeed, during Phase 1 and 2, corresponding to the AP plateau, I_{Kr} was largely inactivated, thus making changes in activation/deactivation inconsequential. Although this is true in guinea-pig myocytes [11], I_{Kr} inactivation may be slightly weaker in the human AP [16], and this might partially unveil the effect of activation/deactivation gating.

Downregulation of channel expression or channel blockade (both represented by g_{max} reduction) are the most common I_{Kr} abnormality underlying QT prolongation [17]; therefore, the relatively small effect of g_{max} changes on APD (Figure 3D) was unexpected. Possibly the g_{max} changes considered here (± 30%) are small as compared to those occurring when QT prolongation is observed. Although g_{max} reduction increased significantly SD1, the latter was not affected by g_{max} increment (Figure 3D). Although the association of I_{Kr} deficiency with increased APD variability is a well-established notion, this asymmetry was unexpected and a further example of how symmetrical changes in channel properties may result in asymmetrical AP responses. SD1/SD2 ratio did not significantly increase in response to decrements in g_{max}; this contrasts with its increment following blockade of native I_{Kr}. Again, this suggests that mI_{Kr} may not be fully representative of native I_{Kr} in terms of sensitivity to the type of perturbations reflected by SD2.

6. Mechanistic interpretation

The AP profile is ultimately determined by a feedback loop linking membrane potential to the many (V-dependent) conductances contributing to total membrane current (I_m). Such a loop is preserved in DC mode; therefore, AP changes after modulation of an individual component of I_m (I_{Kr} in the present case) might be either buffered or boosted by the feedback response of other components. We will refer to this phenomenon as active response of AP to I_{Kr} perturbation. An additional factor to be considered in interpreting the observed effects

is nonlinearity of the relationship between I_m ($\propto$dV/dt) and APD ($\propto(dV/dt)^{-1}$). Being merely numeric, this has been referred to as an intrinsic property of the system, of general value, and independent of the components underlying the active response [18, 19]. A relevant consequence of the intrinsic property is that a given change in I_m is expected to affect APD more if it occurs during a slow phase of repolarization (Figure 5 in Bányász [19]).

During Phase 1, current balance is dominated by the match between noninactivating I_{CaL} and I_{Na} components and I_{Ks} onset, which yields a relatively small I_m, that is, slow repolarization. The fragility of this phase resides precisely in the fact that, being I_m small (in the order of 0.3 pA/pF), it can be easily doubled, or halved, by even minor current changes. Since dV/dt and I_m are linearly related, the same applies to repolarization rate. Thus, high APD sensitivity to I_{Kr} changes occurring in this phase is expected as the consequence of system's intrinsic property [18].

Current theories on the genesis of early-afterdepolarizations (EADs) points to Phase 2 as the one in which active responses are in a more delicate balance. Indeed, in this phase, the outward current surge supported by I_{Kr} matches the inward resurgent components of I_{CaL} and $I_{Na,}$ which are prone to autoregenerative reactivation. Furthermore, rather dramatic changes in subsarcolemmal ionic (Ca^{2+} and Na^{+}) concentrations occur in this phase and even subtle changes in their match with membrane potential may affect the sign and magnitude of the current carried by NCX (Na^{+}/Ca^{2+} exchanger). Thus, we would

expect Phase 2 to be a major source of SD1 through system's active property [12].

With its large dV/dt, resulting from auto-regenerative recovery of inward-rectifying K^+ currents (I_{Kr} and I_{K1}), Phase 3 would be expected to be relatively immune to current perturbations.

Analysis of the patterns shown in Figure 7 is largely, but not entirely, coincident with such theoretical expectations. The only intervention changing APD substantially was modulation of inactivation midpoint ($V_{0.5}I$), that is, the one having a sizable impact on mI_{Kr} during Phase 1. This fulfills the expectation that current changes during slow repolarization may have a larger impact on APD (intrinsic property; see above). The pattern was somewhat different for SD1, which was sensitive also to mI_{Kr} changes during Phase 2 and 3. Notably, APD stabilization (decreased SD1) required mI_{Kr} to increase during Phase 2. Changes in activation/deactivation gating had a negligible effect on APD (Figure 4, 6 and 7B). This is conceivably because they affected I_{Kr} during Phase 3 only, when repolarization rate is high [18, 19]. This interpretation implies that activation/deactivation gating might be more relevant to APD modulation if I_{Kr} inactivation during Phase 1 were less complete, as may be the case in canine and human myocyte [16].

7. Limitations

The whole experimental approach used in this study relies on the assumption that I_{E4031}, on which mI_{Kr} was optimized, accurately

reflects I_{Kr}. This requires E4031 selectivity for I_{Kr} and constancy of E4031 block throughout the electrical cycle. Whereas at the concentration used, E4031 is indeed selective [20], block voltage-dependency might theoretically distort the current profile during the AP. Nevertheless, the kinetics of V-dependent E4031 binding and unbinding are very slow [21], thus ensuring that, once block has achieved steady-state during repetitive depolarization (at physiological CLs), it will remain constant throughout the electrical cycle [22]. I_{E4031} recordings under AP-clamp were obtained under conditions, allowing achievement of steady-state E4031 blockade. Thus, under the present conditions, close similarity between I_{E4031} and I_{Kr} can be reasonably assumed. A further issue is how accurately mI_{Kr} reproduces I_{E4031} properties. In this study mI_{Kr} parameters were optimized on I_{E4031} recorded during AP-clamp. This approach is more stringent than parameter estimation from traditional V-clamp protocols, because the current profile during AP-clamp closely depends on gating kinetic properties that might be otherwise incorrectly estimated. I_{E4031} could be adequately reproduced even if mI_{Kr} included simplifications, performed in the sake of computational speed. Whereas native I_{Kr} inactivates with a time constant in the 1 to 4 ms range, mI_{Kr} inactivation was made instantaneous. Furthermore, mI_{Kr} activation/deactivation kinetics was described by a single exponential. Numeric simulations (Figure I and II in the Data Supplement) showed that these simplifications were indeed inconsequential on repolarization because they affected I_{Kr} slightly and during Phase 3 only.

Generalization of results to other species should consider species-specific aspects of guinea-pig electrophysiology; these include pronounced I_{Kr} inactivation during the plateau phase (discussed above) and strong I_{Ks} expression, which might reduce the impact of I_{Kr} abnormalities.

8. Implications

Identification of the relative impact of I_{Kr} gating properties may provide a new framework for predicting the consequences of I_{Kr} mutations on APD and its variability, 2 quantities strongly associated with arrhythmogenic risk. Although the relative weight of gating components (inactivation versus activation) might be at least partially species-specific, the concept that the impact of a given defect may strictly depend on how it alters I_{Kr} distribution during repolarization (Figure 7) is likely of general value.

The present results point to a surprising lack of APD sensitivity in detecting I_{Kr} abnormalities and identify SD1 as a more sensitive index. This may be relevant to the choice of risk identifiers to be applied in mutation or drug screening. While the prognostic significance of SD1/SD2 awaits to be tested, its suitability to report on the frequency content of variability may help in the identification of the underlying mechanisms.

Being tested in the context of a real guinea-pig myocyte, the outcome of I_{Kr} modulation may represent a reference for validation of guinea-

pig AP numeric models; detection of possible discrepancies would likely provide valuable information for overall model optimization.

Finally, by confirming/challenging theoretical expectations, the present results have refined our interpretation of the complex relation between current and repolarization abnormalities.

Sources of funding

This work has been supported by academic funding (FAR, Fondo di Ateneo per la Ricerca) of the University Milano-Bicocca.

References

1. Zareba W, Bayes dL. *QT dynamics and variability*. Ann Noninvasive Electrocardiol. 2005;10:256-262.

2. Wilders R. *Dynamic clamp: a powerful tool in cardiac electrophysiology*. J Physiol. 2006;576:349-359.

3. Ortega FA, Butera RJ, Christini DJ, White JA, Dorval AD. *Dynamic clamp in cardiac and neuronal systems using RTXI*. Methods Mol Biol. 2014;1183:327-354.

4. Thomsen MB, Oros A, Schoenmakers M, van Opstal JM, Maas JN, Beekman JD, Vos MA. *Proarrhythmic electrical remodelling is associated with increased beat-to-beat variability of repolarisation*. Cardiovasc Res. 2007;73:521-530.

5. Flore V, Willems R. *T-wave alternans and beat-to-beat variability of repolarization: pathophysiological backgrounds and clinical relevance*. Acta Cardiol. 2012;67:713-718.

6. Zaza A, Rocchetti M, Brioschi A, Cantadori A, Ferroni A. *Dynamic Ca^{2+}-induced inward rectification of K^{+} current during the ventricular action potential*. Circ Res. 1998;82:947-956.

7. Luo C-H, Rudy Y. *A dynamic model of the cardiac ventricular action potential. I. Simulation of ionic currents and concentration changes*. Circ Res. 1994;74:1071-1096.

8. Zeng J, Laurita KR, Rosenbaum DS, Rudy Y. *Two components of the delayed rectifier K+ current in ventricular myocytes of the guinea pig type. Theoretical formulation and their role in repolarization*. Circ Res. 1995;77:140-152.

9. Wettwer E, Scholtysik G, Schaad A, Himmel H, Ravens U. *Effects of the new class III antiarrhythmic drug E-4031 on myocardial contractility and electrophysiological parameters*. J Cardiovasc Pharmacol. 1991;17:480-487.

10. Rocchetti M, Besana A, Gurrola GB, Possani LD, Zaza A. *Rate-dependency of delayed rectifier currents during the guinea-pig ventricular action potential*. J Physiol. 2001;534:721-732.

11. Bartolucci C, Altomare C, Bennati M, Furini S, Zaza A, Severi S. *Combined action potential- and dynamic-clamp for accurate computational modelling of the cardiac IKr current*. J Mol Cell Cardiol. 2015;79:187-194.

12. Heijman J, Zaza A, Johnson DM, Rudy Y, Peeters RL, Volders PG, Westra RL. *Determinants of beat-to-beat variability of repolarization duration in the canine ventricular myocyte: a computational analysis*. PLoS Comput Biol. 2013;9:e1003202.

13. Thomsen MB, Verduyn SC, Stengl M, Beekman JD, de Pater G, van Opstal J, Volders PG, Vos MA. *Increased short-term variability of repolarization predicts d-sotalol-induced torsades de pointes in dogs*. Circulation. 2004;110:2453-2459.

14. Brugada R, Hong K, Dumaine R, Cordeiro J, Gaita F, Borggrefe M, Menendez TM, Brugada J, Pollevick GD, Wolpert C, Burashnikov E, Matsuo K, Wu YS, Guerchicoff A, Bianchi F, Giustetto C, Schimpf R, Brugada P, Antzelevitch C. *Sudden death associated with short-QT syndrome linked to mutations in HERG*. Circulation. 2004;109:30-35.

15. Shao C, Lu Y, Liu M, Chen Q, Lan Y, Liu Y, Lin M, Li Y. *Electrophysiological study of V535M hERG mutation of LQT2*. *J* Huazhong Univ Sci Technolog Med Sci. 2011;31:741-748.

16. Jost N, Virag L, Comtois P, Ordog B, Szuts V, Seprenyi G, Bitay M, Kohajda Z, Koncz I, Nagy N, Szel T, Magyar J, Kovacs M, Puskas LG, Lengyel C, Wettwer E, Ravens U, Nanasi PP, Papp JG, Varro A, Nattel S. *Ionic mechanisms limiting cardiac repolarization reserve in humans compared to dogs*. J Physiol. 2013;591:4189-4206.

17. Mehta A, Sequiera GL, Ramachandra CJ, Sudibyo Y, Chung Y, Sheng J, Wong KY, Tan TH, Wong P, Liew R, Shim W. *Re-trafficking of hERG reverses long QT syndrome 2 phenotype in human iPS-derived cardiomyocytes*. Cardiovasc Res. 2014;102:497-506.

18. Zaza A. Control of the cardiac action potential: *The role of repolarization dynamics*. J Mol Cell Cardiol. 2010;48:106-111.

19. Banyasz T, Horvath B, Virag L, Barandi L, Szentandrassy N, Harmati G, Magyar J, Marangoni S, Zaza A, Varro A, Nanasi PP. *Reverse rate dependency is an intrinsic property of canine cardiac preparations*. Cardiovasc Res. 2009;84:237-244.

20. Sanguinetti MC, Jurkiewicz NK. *Two components of cardiac delayed rectifier K+ current. Differential sensitivity to block by class III antiarrhythmic agents*. J Gen Physiol. 1990;96:195-215.

21. Spector PS, Curran ME, Keating MT, Sanguinetti MC. *Class III antiarrhythmic drugs block HERG, a human cardiac delayed rectifier K+ channel. Open-channel block by methanesulfonanilides*. Circ Res. 1996;78:499-503.

22. Hancox JC, Levi AJ, Witchel HJ. *Time course and voltage dependence of expressed HERG current compared with native "rapid" delayed rectifier K current during the cardiac ventricular action potential*. Pflügers Arch. 1998;436:843-853.

SUPPLEMENTAL MATERIAL

Supplement to Introduction

Clinical KCNH2 mutations with gating abnormalities

The prevailing I_{Kr} abnormality underlying QT prolongation is reduced membrane channel density, modelled in this study by changes in g_{max} (see manuscript Figure 3). However, mutations leading to changes in I_{Kr} gating have also been reported and are the rule in short QT syndromes (Table S1). As shown in Table S1, in many cases the gating abnormality, identified as potentially responsible for QT prolongation, concerns "activation" gating. This is in apparent contrast with the findings of the present study, in which "activation" abnormalities are shown to have minor effects on APD. On one hand, a larger weight of activation/deactivation abnormalities in humans might depend on weaker I_{Kr} inactivation during the AP plateau (see manuscript for discussion). On the other, it should be considered that 1) functional characterization of mutations in heterologous systems at room temperature has obvious limitations; 2) attribution of the phenotype to faster deactivation was based in the best case 1 on an entirely numerical AP model and in the others 2,3 largely conjectural.

Table S1: **KCNH2 mutations including channel gating abnormalities** (reduced channel expression also present in some of them) described in patients with Long- or Short- QT syndromes. The functional abnormality identified as potentially responsible for the electrical phenotype is also listed.

Table S1: **KCNH2 mutations including channel gating abnormalities**

KCNH2 mutation	Clinical Phenotype	Putative pathogenetic gating defect	reference
R531Q	LQT	Positive shift and acceleration of deactivation	[1]
R531W	LQT	Positive shift and acceleration of deactivation	[1]
V535M	LQT	Negative inactivation shift with slowed recovery	[4]
K28E	LQT	Negative inactivation shift	[5]
F29L	LQT	Faster deactivation	[2]
N33T	LQT	Faster deactivation	[2]
R56Q	LQT	Faster deactivation	[2]
M124R	LQT	Faster deactivation	[3]
H70R	LQT	Altered trafficking + faster deactivation	[2]
L86R	LQT	Faster deactivation	[2]
N588K	SQT	Positive inactivation shift	[6]

Supplement to Methods

Table S2. mI_{Kr} parameters: g_{max} = maximal conductance; $V_{0.5}A$ and *sA*= mid-potential and slope factor for steady-state activation; $V_{0.5}I$ and *sI* = mid-potential and slope factor for steady-state inactivation; τ = maximal value of the voltage-dependent activation/deactivation time-constant.

Table S2. mI_{Kr} parameters

	mI_{Kr}
g_{max}	0.03 mS/µF
$V_{0.5}A$	-20.6 mV
sA	5 mV
$V_{0.5}I$	-30.7 mV
sI	14 mV
$\tau_{act/deac}$	270 ms

Table S3. Recording solutions

	Extracellular Tyrode's solution	Intracellular Pipette solution
NaCl (mM)	154	
KCl (mM)	4	23
K^+-aspartate (mM)		110
$CaCl_2$ (mM)	2	0.2
$MgCl_2$ (mM)	1	3
HEPES-NaOH (mM)	5	
HEPES-KOH (mM)		5
EGTA-KOH (mM)		0.5
D-glucose (mM)	5.5	
GTP-Na^+ salt (mM)		0.4
ATP-Na^+ salt (mM)		5
Creatine-P- Na^+ salt (mM)		5
pH	7.35	7.3

Effect of gating kinetics on modelled I_{Kr}

The impact of inactivation time-dependency on mI_{Kr} was tested by numerical simulations. To this end, inactivation kinetics was introduced in mI_{Kr}; dependency of inactivation time constant (τ) on membrane potential, shown in Fig S1A, was simulated according to previous estimates supported by experimental results, obtained in the guinea pig at physiological temperature [7]. Fig S1B compares mI_{Kr} profiles with instantaneous and time-dependent inactivation during an AP. The difference between the two models is limited to a small difference in peak current. Since this difference occurred during AP Phase 3, its impact on APD is expectedly small (see manuscript). This expectation was tested by adding either of the two mI_{Kr} versions (with instantaneous or time-dependent inactivation) to "total membrane current" density (I_m), obtained by differentiation of an AP waveform. New AP profiles were then calculated by numerical integration of I_m traces containing the two mI_{Kr} versions respectively. Figure S1C shows that mI_{Kr} inactivation time-dependency had no visible effect on I_m profile, and caused only a minor (3 ms) prolongation of APD at 90% repolarization (visible as slight "thickening" of the AP trace). A similar approach was used to test for the effect of inactivation time-dependency on the outcome of changes in activation rate. The results (not shown) were again suggestive of a minor impact of inactivation time-dependency.

Overall, these simulations indicate that omission of inactivation time-dependency from the mI_{Kr} formulation should not impact significantly on the outcome of DC studies. Nevertheless, it should be

considered that, whereas voltage and current interact in close-loop during a true AP, the present simulations tested only the primary effect of current changes on potential course (open-loop condition). Therefore, they do not rule out the importance of inactivation time-dependency, particularly if slowed by gating abnormalities.

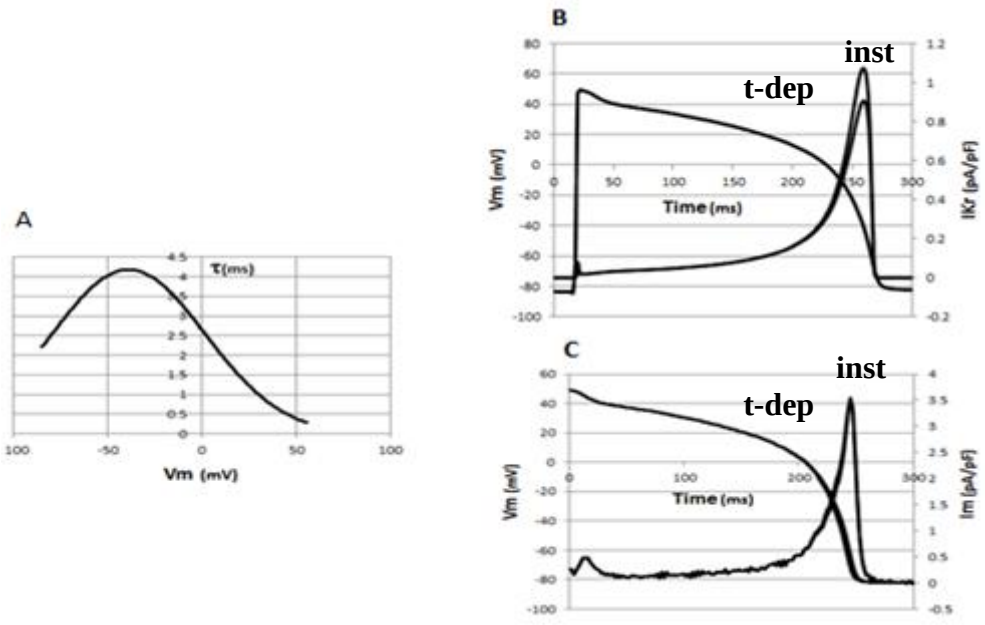

Figure S1: Effect of inactivation time-dependency on mI_{Kr}. A) voltage dependency of the inactivation time constant (τ) incorporated into the model; **B)** comparison between mI_{Kr} (right scale) with instantaneous (inst) or time-dependent (t-dep) inactivation during the AP course (left scale); **C)** total membrane current (I_m) and AP tracings containing mI_{Kr} with either inst or t-dep inactivation.

Whereas I_{Kr} deactivation is reportedly biexponential, in mI_{Kr} activation/deactivation kinetics was described by a single exponential. To test the impact of a slow deactivation component we performed the

simulations shown in Figure S2. Adding the slow kinetic component slightly increased peak I_{Kr}, but had negligible effect on APD. Persistence of a fraction of activated channels during diastole would result in "accumulation" of open state at short diastolic interval; however, also this would be irrelevant because, as shown on the plot of gating variables, 100% of channels activate very early during repolarization even in the absence of the slow component.

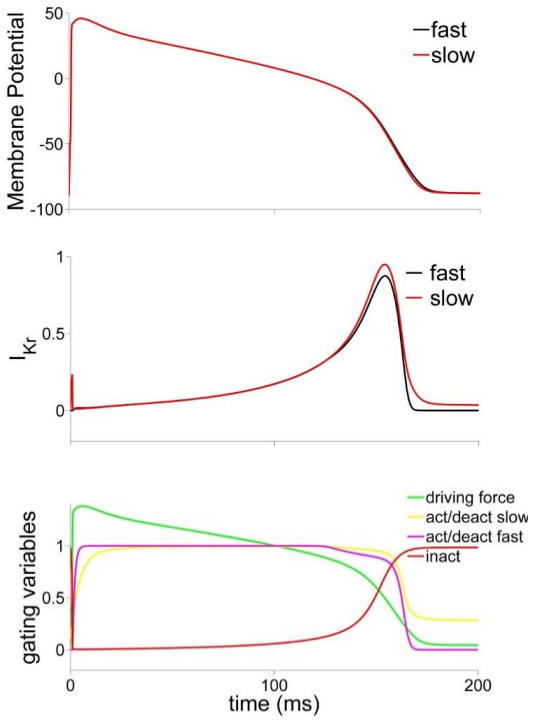

Figure S2: The simulation was performed with the Luo-Rudy AP model in which the original I_{Kr} formulation was replaced by mI_{Kr} (the formulation used in our work). mI_{Kr} was used in two versions: 1) the original one, with activation/deactivation represented as a single exponential (act/deact fast); 2) with activation/deactivation represented as a sum of 2 exponentials as in the human O'Hara-Rudy model [8] (act/deact slow).

Interpretation of SD1, SD2 and SD1/SD2 indexes of variability

SD1 (a.k.a. "Short Term Variability") and SD2 (a.k.a "Long Term Variability") are indexes of temporal variability, initially applied to the analysis of heart rate and more recently applied to repolarization. In previous work [9-11], whereas SD1 was used to quantify "beat-to-beat" variability, SD2 was assumed to reflect variability occurring over a larger number of beats; however, the specificity of these terms was never addressed. In order to clarify the meaning of SD1 and SD2 in terms of variability dynamics, we have tested their performance in a numerical model of variability. The model consisted in a series of 300 values (Y, with mean = 300) in which variability (V) was introduced by a sinus function of adjustable amplitude and frequency. V was generated to oscillate symmetrically around mean Y. In V, the number of beats (N_{beats}) over which Y changes monotonically (i.e. the sinus value goes from 0 to 1) is inversely proportional to the frequency (*f*) of the sinus wave. Figure S3A shows the results of a simulation in which was set to f = 0.3 degr/beat, to analyze the case of a fully monotonic variation of Y over the sampled interval (N_{beats} = 300). While SD1 was much smaller than SD2 in this case (see below), both indexes showed the same dependency on perturbation amplitude, as demonstrated by constancy of SD1/SD2 (multiplied by 10 to make it compatible with figure scales). While f = 0.3 is an extreme case, independency of SD1/SD2 from V amplitude held true at all f values (not shown). These simulations lead to the conclusion that 1) being as affected as SD2 by variations over a large N_{beats}, SD1 does not selectively detect changes in short-term variability ("STV" and "LTV"

are actually misnomers for SD1 and SD2 respectively); 2) the SD1/SD2 ratio is instead insensitive to the amplitude of variability. Figure S3B shows that SD1/SD2 is instead a function of *f*, becoming larger as the latter is increased. Therefore, SD1/SD2 specifically reflects the "frequency content" of V, being large when short-term variability prevails over long-term one (it becomes infinite in the extreme case of true alternans). Figure S3C shows Poincaré plots for three specific cases: a) with f = 0.3 (N_{beats} = 300) data points almost overlap the identity line and SD1/SD2 approaches 0; b) with f = 90, N_{beats} = 4 (e.g in the cycle 0, 1, 0, -1…) and Poincaré plot forms a square, yielding SD1/SD2 = 1; c) In the special case of pure "alternans" (f =180), N_{beats} = 2 (e.g. -1, 1…), points cluster in 2 positions only, Poincaré plot forms a line orthogonal to the identity one, SD2 is null and SD1/SD2 = ∞. This analysis leads to the conclusion that 1) SD1 and SD2 report on changes of variability amplitude, irrespective of its frequency content; 2) the SD1/SD2 ratio is insensitive to variability amplitude, but specifically reflects its frequency content, i.e. it is suitable to discriminate between short-term and long-term variability.

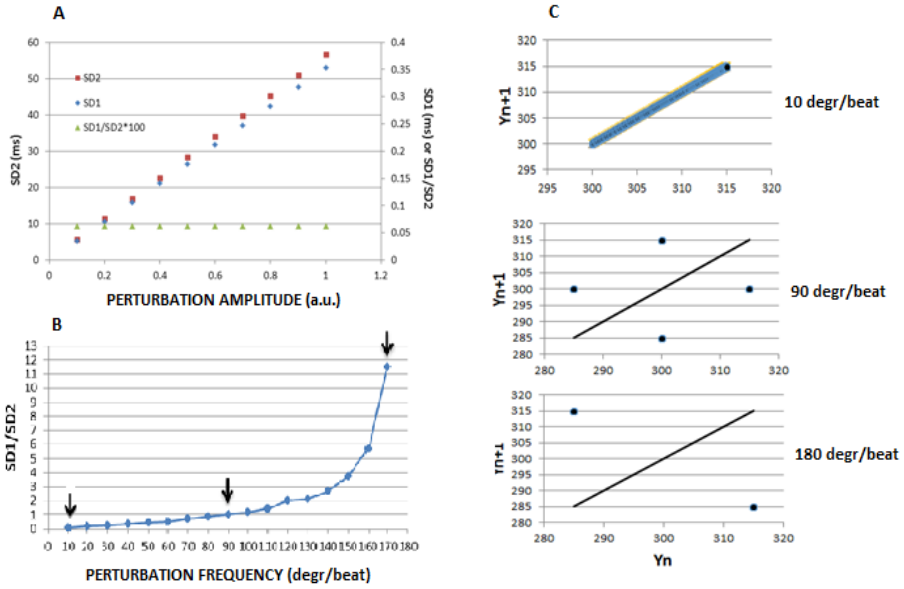

Figure S3: **Variability indexes vs variability properties. A)** dependency of SD2 (left scale), SD1 and SD1/SD2 (right scale, SD1/SD2 multiplied by 10) on variability amplitude; **B)** dependency of SD1/SD2 on variability frequency (*f*); **C)** Poincaré plots at 3 frequency points, corresponding to arrows in panel B. Note that in the upper panel, while visually overlapping the identity line, data points are slightly above it.

Supplement to Results

I_{E4031} replacement by mI_{Kr} at various cycle lengths

Adequacy of mI_{Kr} in replacing the native current was also tested at CLs of 250 ms and 3000 ms within the same myocyte. As shown in Fig S4, APD and SD1 increments induced by E4031 were maximal at CL 1000 ms, which represents a condition of marked bradycardia in the guinea-pig. On the other hand, mI_{Kr} ability to revert E4031-

induced changes was similar at all CLs, thus indicating adequacy of the current model under different AP profiles. We also evaluated the time course of APD adaptation when switching from the shorter to the longer CL. An initial APD shortening in the first several cycles, the ensuing APD prolongation was well fitted by a single exponential. E4031 tended to emphasize the initial shortening and to prolong the time constant (τ) of adaptation, but the changes did not achieve statistical significance. All E4031-induced changes were reversed by mI_{Kr} injection.

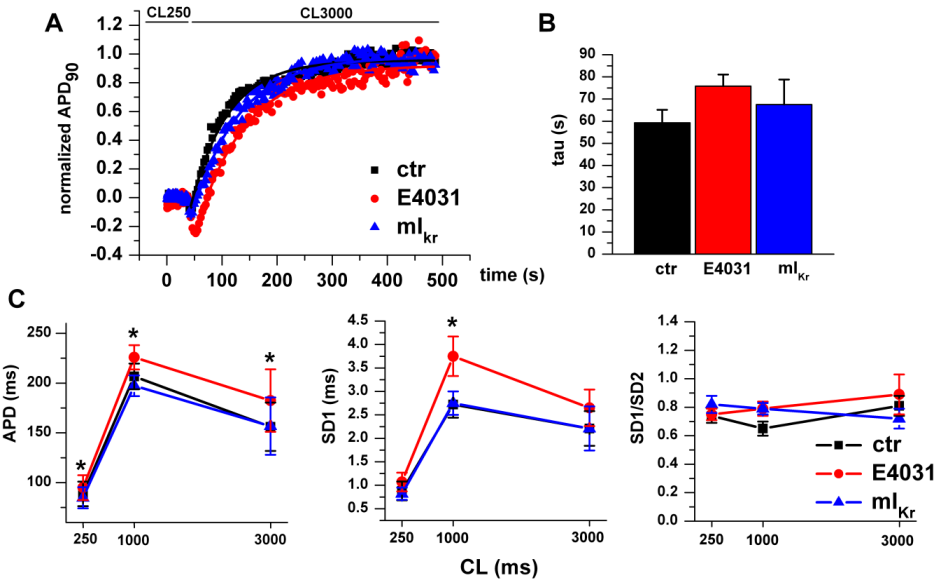

Figure S4: I_{E4031} replacement by mI_{Kr} at various cycle lengths. A) Time course of APD adaptation when switching from the shorter (250 ms) to the longer (3000 ms) CL. APD values were normalized to the steady-state values recorded at CL3000 for clarity. **B)** Statistics of the time constant (tau) of adaptation ($n \geq 6$). **C)** Statistics of APD, SD1 and SD1/SD2 in all experimental conditions (*P<0.05 vs ctr; $n \geq 5$).

Effect of $V_{0.5}A$ changes without concomitant shifts in τ curve

According to simple reaction kinetics, shifts in the distribution of states at equilibrium may be associated to similar shifts in the velocity of transitions between states. Therefore, the data concerning $V_{0.5}A$ changes reported in the manuscript (Figure 4) were generated by concomitantly shifting V-dependency of activation time constants (τA). The less likely alternative condition, in which shifts in steady-state activation occur without concomitant changes in V-dependency of τA was tested in a separate series of experiments and is presented in Figure S5. Shifts in $V_{0.5}A$ alone slightly modified mI_{Kr} profile and V-dependency (Figure S5D) during late repolarization (Phase 3), but failed to affect APD and its variability (Figure S5E).

Fig. S3

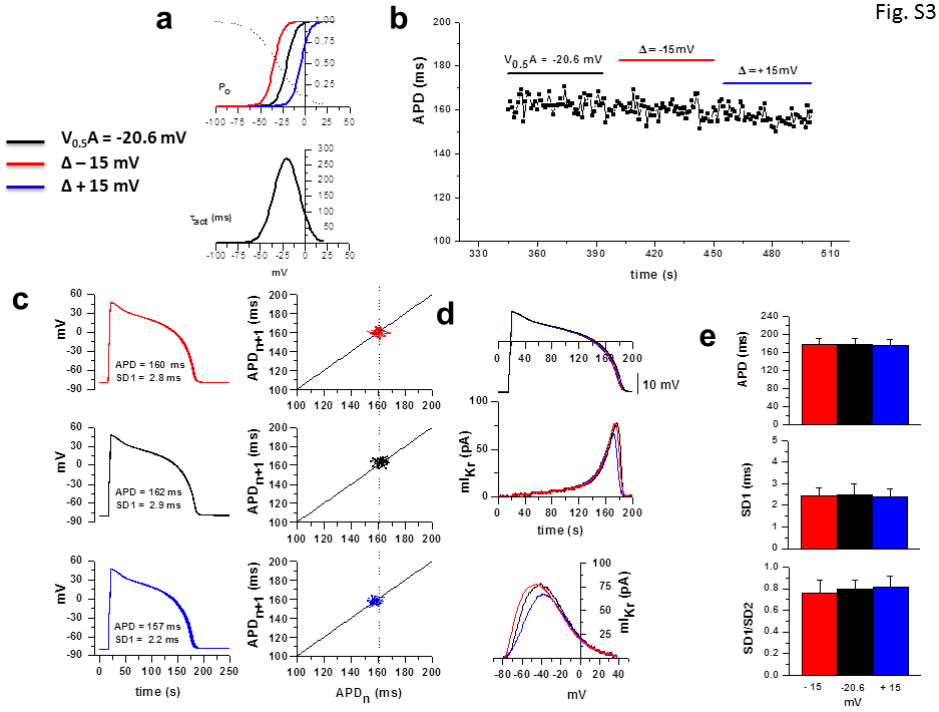

Figure S5: Effect of $V_{0.5}A$ changes without shifts in τ curve. Recordings performed at $V_{0.5}A$ = -20.6 mV and with Δ ± 15 mV are shown as: **a)** Steady-state activation (P_o) computed by the model in three conditions (colour) and superimposed inactivation curve (dotted line); below $\tau_{act/deact}$ curve in black line; **b)** representative time course of APD recorded at three values of $V_{0.5}A$; **c)** example of 10 APs for each conditions with relative APD and SD1 values and Poincaré plot at the right of panel; ctr APD is evidenced as dot line; **d)** mI_{Kr} profile aligned with the corresponding average AP waveform represented as I/t and I/V_m plots; **e)** statistics of APD, SD1 and SD1/SD2 in all experimental conditions (NS; n=7).

Supplemental References

1. McBride CM, Smith AM, Smith JL, Reloj AR, Velasco EJ, Powell J, Elayi CS, Bartos DC, Burgess DE, Delisle BP. *Mechanistic basis for type 2 long QT syndrome caused by KCNH2 mutations that disrupt conserved arginine residues in the voltage sensor*. J Membr Biol. 2013;246:355-364.

2. Chen J, Zou A, Splawski I, Keating MT, Sanguinetti MC. *Long QT syndrome-associated mutations in the Per-Arnt-Sim (PAS) domain of HERG potassium channels accelerate channel deactivation*. J Biol Chem. 1999;274:10113-10118.

3. Shushi L, Kerem B, Goldmit M, Peretz A, Attali B, Medina A, Towbin JA, Kurokawa J, Kass RS, Benhorin J. *Clinical, genetic, and electrophysiologic characteristics of a new PAS-domain HERG mutation (M124R) causing Long QT syndrome*. Ann Noninvasive Electrocardiol. 2005;10:334-341.

4. Shao C, Lu Y, Liu M, Chen Q, Lan Y, Liu Y, Lin M, Li Y. *Electrophysiological study of V535M hERG mutation of LQT2*. *J* Huazhong Univ Sci Technolog Med Sci. 2011;31:741-748.

5. Rossenbacker T, Mubagwa K, Jongbloed RJ, Vereecke J, Devriendt K, Gewillig M, Carmeliet E, Collen D, Heidbuchel H, Carmeliet P. *Novel mutation in the Per-Arnt-Sim domain of KCNH2 causes a malignant form of long-QT syndrome*. Circulation. 2005;111:961-968.

6. McPate MJ, Duncan RS, Milnes JT, Witchel HJ, Hancox JC. *The N588K-HERG K+ channel mutation in the 'short QT syndrome': mechanism of gain-in-function determined at 37 degrees C*. Biochem Biophys Res Commun. 2005;334:441-449.

7. Rocchetti M, Besana A, Gurrola GB, Possani LD, Zaza A. *Rate-dependency of delayed rectifier currents during the guinea-pig ventricular action potential*. J Physiol. 2001;534:721-732.

8. O'Hara T, Virag L, Varro A, Rudy Y. *Simulation of the undiseased human cardiac ventricular action potential: model formulation and experimental validation*. PLoS Comput Biol. 2011;7:e1002061.

9. Brennan M, Palaniswami M, Kamen P. *Do existing measures of Poincare plot geometry reflect nonlinear features of heart rate variability?* IEEE Trans Biomed Eng. 2001;48:1342-1347.

10. Johnson DM, Heijman J, Bode EF, Greensmith DJ, van der LH, Abi-Gerges N, Eisner DA, Trafford AW, Volders PG. *Diastolic spontaneous calcium release from the sarcoplasmic reticulum increases beat-to-beat variability of repolarization in canine ventricular myocytes after beta-adrenergic stimulation*. Circ Res. 2013;112:246-256.

11. Heijman J, Zaza A, Johnson DM, Rudy Y, Peeters RL, Volders PG, Westra RL. *Determinants of beat-to-beat variability of repolarization duration in the canine ventricular myocyte: a computational analysis*. PLoS Comput Biol. 2013;9:e1003202.

Chapter 4

Summary and conclusions

The first study was focused on the analysis of the effects of changes in NOS1 activity on SR functional stability, repolarization and arrhythmogenesis in the context of I_{Ks} deficiency, to mimic repolarization defect characteristic of LQT1 phenotype. This work demonstrated that in this specific experimental setting, NOS1 down-regulation contributes to APD prolongation and enhance Ca^{2+} influx (through enhancement of I_{CaL}), and these effects may compromise SR stability in the presence of adrenergic stimulation. Moreover, our study further suggested that in a circumstance of altered NOS1 activity, the duration of AP is important for the occurrence of those sings of SR instability. This finding is of a certain implication in a context in which repolarization is prolonged as a consequence of the loss of function of I_{Ks} in LQT1 patients. All together, these potential arrhythmogenic effects of NOS1 inhibition could be paralleled to the increased incidence of SCD in LQT1 patients carrying NOS1AP polymorphisms, suggesting that they may lead to loss of NOS1 function. To demonstrate this link between NOS1AP SNPs and NOS1 dysregulation, the next step will be the evaluation of NOS1 function in patient's specific induced pluripotent stem cell-derived cardiomyocytes (iPSC-CMs) carrying the LQT1 mutation with different NOS1AP SNPs.

The second project exploited Dynamic Clamp (DC) to systematically analyze the effect of changes in I_{Kr} conductance and gating properties on guinea pig APD and its time-variability, an index of electrical instability. The results provided by this work might be instrumental to risk assessment and clinical management of I_{Kr} mutations (like in type 2 Long-QT syndrome), as abnormalities of this current are associated with remarkable prolongation and instability of repolarization, conditions that involved arrhythmogenic risk. Moreover, this work may be relevant to the choice of risk identifiers to be applied in mutation or drug screening.

The translational relevance of these studies relies mainly in providing a further understanding of the mechanisms underlying repolarization abnormalities in the context of the two prevalent Long QT syndrome's types, LQT1 and LQT2. These results may be helpful in identifying targets for arrhythmia prevention and biomarkers suitable to risk stratification in conditions leading to sudden cardiac death.

Chapter 5

Published papers

1. Ronchi C, Torre E, Rizzetto R, Sala L, **Bernardi J**, Mostacciuolo G, Rocchetti M, Zaza A. *Late Sodium Current and intracellular ionic homeostasis in acute ischemia***.** Basic Res Cardiol, 2017;112(2):12.

2. Altomare C, Bartolucci C, Sala L, **Bernardi J**, Mostacciuolo G, Rocchetti M, Severi S, Zaza A. *IKr impact on repolarization and its variability assessed by Dynamic Clamp*. Circ Arrhythm Electrophysiol. 2015;8(5):1265-75.